



## Recent glaciation at high elevations on Arsia Mons, Mars: Implications for the formation and evolution of large tropical mountain glaciers

David E. Shean,<sup>1,2</sup> James W. Head III,<sup>1</sup> James L. Fastook,<sup>3</sup> and David R. Marchant<sup>4</sup>

Received 31 May 2006; revised 24 August 2006; accepted 26 October 2006; published 21 March 2007.

[1] The  $\sim 166,000$  km<sup>2</sup> fan-shaped deposit at Arsia Mons contains three characteristic facies (ridged, knobby, and smooth), which are interpreted as the depositional remains of a cold-based glacier that was present on the west–northwestern flanks in the Late Amazonian period of Mars history. Here, we consider several high-elevation graben on the western flank of Arsia Mons that are interpreted as the source regions for late-stage, cold-based glaciers that overflowed graben walls, advanced tens to hundreds of kilometers downslope, experienced subsequent retreat, and left distinctive depositional features similar to those associated with cold-based glaciers in the Dry Valleys of Antarctica. These new observations provide additional support for a cold-based glacial interpretation of the Tharsis Montes fan-shaped deposits. Morphological evidence suggests that the largest of these graben was the primary source region for the most proximal smooth facies lobes at Arsia Mons, and map-plane ice sheet reconstructions are consistent with these observations. This relationship has significant implications for the relative ages of the individual facies within the fan-shaped deposit, including the possibility that the smooth facies represents several distinct phases of glaciation. The high relief and large elevation differences between the upslope and downslope walls of these graben appear to be critical factors for ice accumulation and the generation/collection of rockfall within glacial accumulation zones. We suggest that rockfall was the dominant process responsible for debris-cover formation on the glaciers sourced within these graben and consider the implications for the entire Arsia fan-shaped deposit. New crater count data suggest that the fill material in the large Arsia graben formed within the past  $\sim 100$  Myr (model age of  $\sim 65$  Ma). Taken together, these new observations provide additional evidence for several periods of Late Amazonian climate change on Mars within the past few 100 Myr resulting in episodes of tropical mountain glaciation. Finally, MOLA topography reveals that several lobate features interpreted as remnant debris-covered ice from the most recent phase of glaciation are presently hundreds of meters thick, suggesting the possibility of long-term, near-surface water ice survival in the equatorial regions of Mars.

**Citation:** Shean, D. E., J. W. Head III, J. L. Fastook, and D. R. Marchant (2007), Recent glaciation at high elevations on Arsia Mons, Mars: Implications for the formation and evolution of large tropical mountain glaciers, *J. Geophys. Res.*, *112*, E03004, doi:10.1029/2006JE002761.

### 1. Introduction

[2] Over the past several decades, high-resolution images of the Martian surface have revealed intriguing nonpolar

features attributed to flow or relaxation of volatile-rich material. These include, but are not limited to, lobate debris aprons [Squyres, 1979, 1989; Colaprete and Jakosky, 1998; Mangold, 2003; Perron *et al.*, 2003a; Chuang and Crown, 2005], concentric crater fill [Squyres and Carr, 1986; Carr, 1996; Berman *et al.*, 2005], lineated valley fill [Lucchitta, 1984; Carr, 2001; Head *et al.*, 2005a, 2006], viscous flow-like features [Milliken *et al.*, 2003], and other lobate features interpreted as rock glaciers [Degenhardt and Giardino, 2003; Whalley and Azizi, 2003] or debris-covered glaciers [Head and Marchant, 2003; Arfstrom and Hartmann, 2005; Hauber *et al.*, 2005; Shean *et al.*, 2005]. These features are distributed over low latitudes to midlatitudes and all appear to have experienced flow due to the presence of volatiles

<sup>1</sup>Department of Geological Sciences, Brown University, Providence, Rhode Island, USA.

<sup>2</sup>Now at Department of Earth Science, Boston University, Boston, Massachusetts, USA.

<sup>3</sup>Department of Computer Science, University of Maine, Orono, Maine, USA.

<sup>4</sup>Department of Earth Science, Boston University, Boston, Massachusetts, USA.

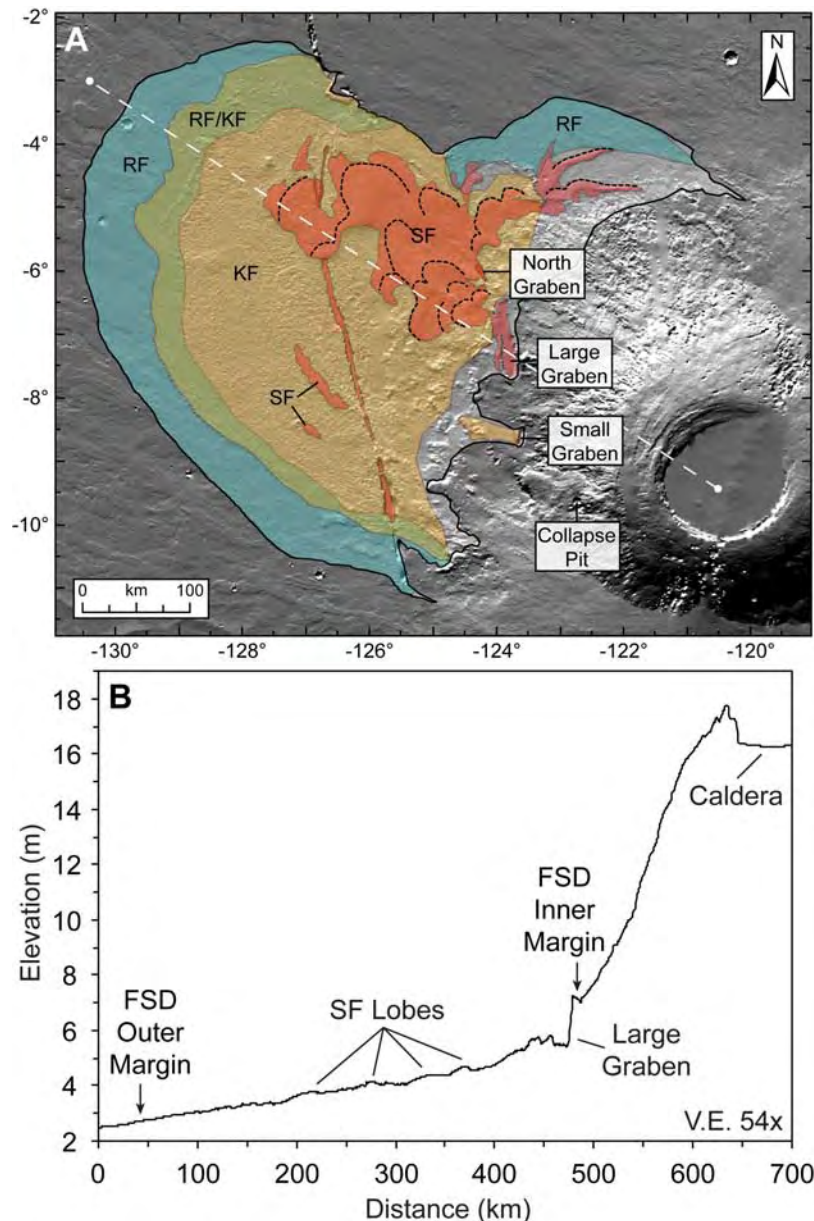


**Figure 1.** (a) Regional context for the Arsia Mons fan-shaped deposit. MOLA shaded relief basemap (illumination from the NNW) with the fan-shaped deposit outlined by thick black line. The three main facies of the fan-shaped deposits, the ridged facies (RF, blue), the knobby facies (KF, gold), and the smooth facies (SF, red) are mapped. Dashed black lines within the smooth facies represent major smooth facies lobes apparent in MOLA gridded data. The high-elevation features discussed in this work are labeled as large graben, north graben, small graben, and collapse pit. Note the roughly north–south trend of the large graben that cuts through the central regions of the fan-shaped deposit and also the generally parallel nature of the high-elevation graben. The white circles and dashed line provide context for the profile in Figure 1b. (b) MOLA topography extracted from 128 pixel/degree gridded data with a spacing of  $\sim 650$  m. The solid arrows delineate the extent of the fan-shaped deposit. Note the high elevation and relief of the eastern wall of the large graben relative to the western wall. Also note the position of the large graben at the intersection of the shallow regional slope of the plains to the west–northwest of Arsia Mons ( $\sim 0$ –475 km) with the steeper slopes on the flanks of the main edifice ( $\sim 475$ –625 km).

(most likely water ice), although the absolute volatile content for each is widely disputed.

[3] Near the equator, each of the three Tharsis Montes has a large fan-shaped deposit on the west–northwestern flanks [Williams, 1978; Lucchitta, 1981; Zimbelman and Edgett,

1992; Head and Marchant, 2003; Shean et al., 2005]. The  $\sim 166,000$  km<sup>2</sup> deposit at Arsia Mons (Figure 1) is the largest of the three and contains the best examples of the characteristic deposit morphology. Our previous work suggests that the fan-shaped deposits represent the deposi-

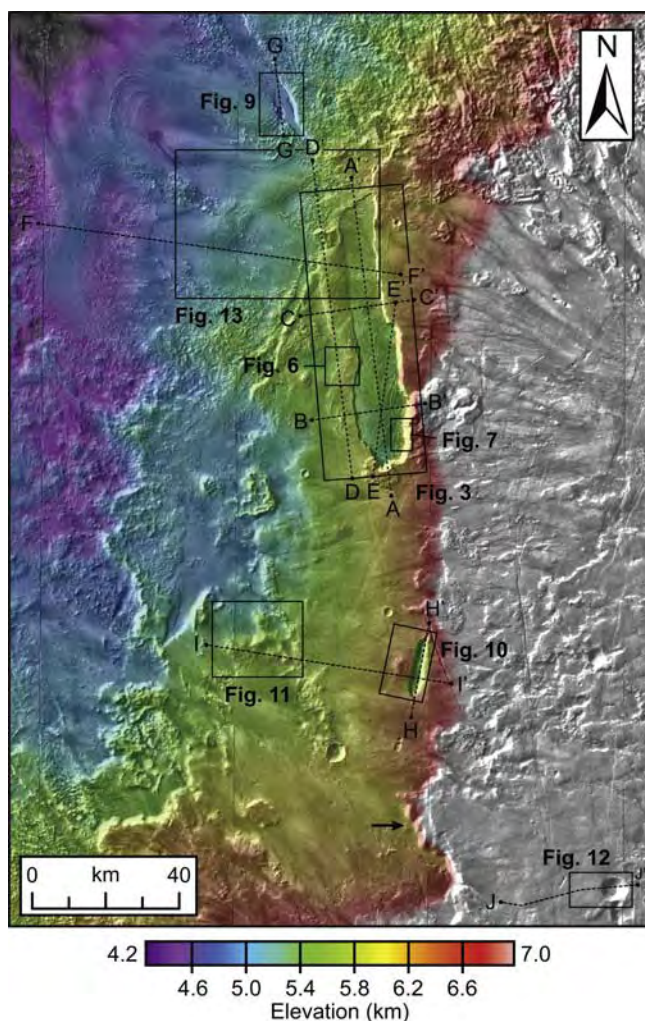


**Figure 2.** MOLA 128 pixel/degree gridded topography data over HRSC basemap. Location of figures (solid black boxes); dashed lines with labels show location of profiles in Figures 5, 9, 10, and 12. Solid black arrow near the bottom center of the image points to high-relief scarp with no evidence of associated glacial activity. Note the topography and position of the most proximal smooth facies lobes with respect to the large graben.

tional remains of cold-based mountain glaciers that formed on the west–northwestern flanks of the edifices during the late Amazonian period of Mars history [Head and Marchant, 2003; Parsons and Head, 2004; Shean et al., 2005]. Previously proposed and alternative hypotheses for the fan-shaped deposits are outlined by Zimbelman and Edgett [1992] and reevaluated by Shean et al. [2005].

[4] The fan-shaped deposits are composed of three main facies (Figure 1): ridged, knobby and smooth [Lucchitta, 1981; Zimbelman and Edgett, 1992; Scott and Zimbelman, 1995; Scott et al., 1998; Head and Marchant, 2003; Shean et al., 2005], which are interpreted to represent deposition during different phases of cold-based glacial activity. We interpret the outermost ridged facies as drop moraines deposited around the margins of a relatively stable, retreating cold-based glacier [Head and Marchant, 2003; Parsons

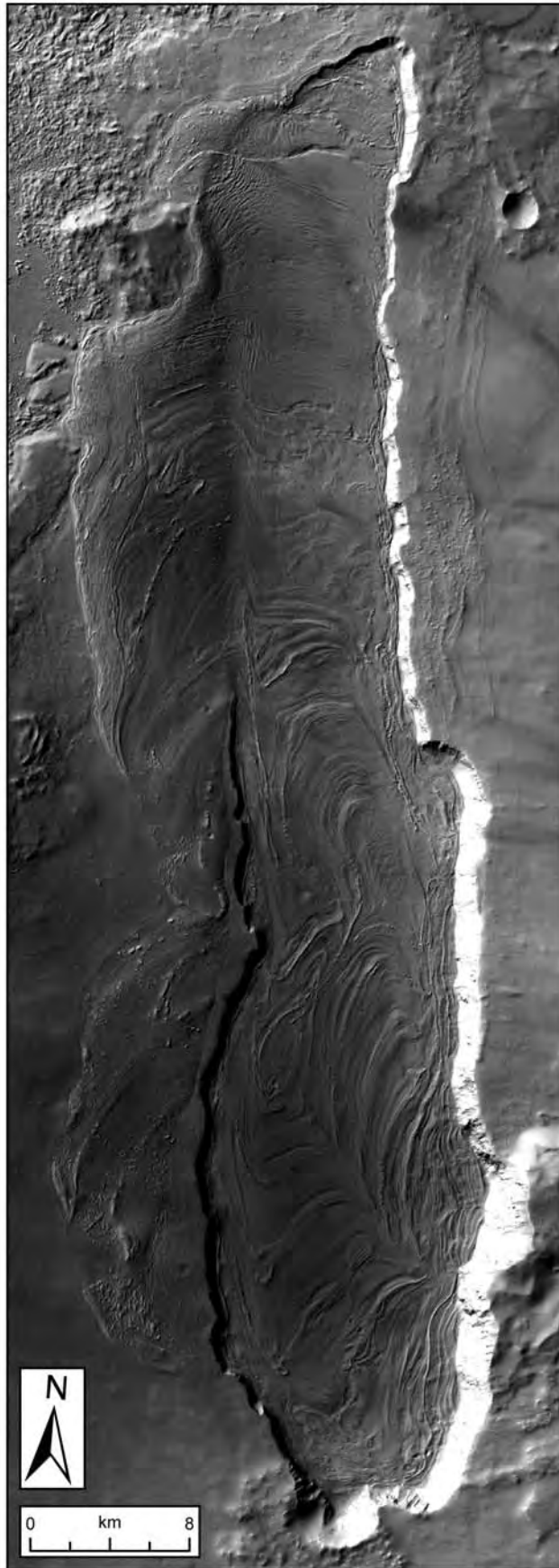
and Head, 2004; Shean et al., 2005]. The more medial knobby facies is interpreted as a sublimation till formed due to changing climate conditions that led to collapse and downwasting of the ice sheet after deposition of the outer ridged facies. Finally, the smooth facies is interpreted as debris-covered glaciers that may represent (1) the final waning stages of glaciation associated with the large mountain glaciers, (2) resurgence of glaciation under climatic conditions that produced more limited deposits, or (3) some combination of these two [Head and Marchant, 2003; Shean et al., 2005].

[5] The smooth facies at Arsia Mons consists of nearly a dozen, ~20–100 km long, lobate, smooth-surfaced features, that are tens to hundreds of meters thick, with concentric arcuate surface ridges near their margins (Figures 1 and 2) [Head and Marchant, 2003; J. W. Head et al., The Arsia Mons fan-shaped deposit: New evidence supporting a cold-based glacial model, manuscript in preparation, 2007 (hereinafter referred to as Head et al., manuscript in preparation, 2007)]. Stratigraphically, these lobes are the youngest features within the deposits [Lucchitta, 1981; Zimbelman and Edgett, 1992; Head and Marchant, 2003] and they cover an area of ~24,000 km<sup>2</sup> at Arsia (Figure 1). In plan view, the most proximal smooth facies lobes display relatively thin necks originating at higher elevations, with broader distal toes at lower elevations (Figure 2). In addition, MOLA topography shows that the individual lobes display thick distal margins that extend downward from “spoon-shaped hollows” and medial depressions [Head and Marchant, 2003; Head et al., manuscript in preparation, 2007]. The surface morphology of the more distal smooth facies lobes also appears more degraded than the most proximal lobes.

[6] On the basis of Viking data, the smooth facies at Arsia and Pavonis Mons was interpreted to represent rock glacier deposits [Lucchitta, 1981], pyroclastic/ash flows [Zimbelman and Edgett, 1992; Scott and Zimbelman, 1995; Scott et al., 1998] and piedmont-like debris-covered glaciers [Head and Marchant, 2003; Shean et al., 2005; Head et al., manuscript in preparation, 2007]. Similar features near the west–northwestern basal scarp at Olympus Mons [Lucchitta, 1981] have also been interpreted as debris-covered glaciers and their depositional remains [Neukum et al., 2004; Head et al., 2005a; Milkovich et al., 2006].

[7] Although extensive evidence suggests that glaciation was responsible for the formation of the smooth facies, the exact processes of emplacement and evolution are not well understood. Additional questions remain unanswered, including (1) the location and nature of the accumulation zones for these glaciers and (2) how these are related to the emplacement of the more extensive mountain glacial deposits.

[8] Earlier studies of the Arsia fan-shaped deposit by Lucchitta [1981] and Scott and Zimbelman [1995] noted that some of the smooth facies lobes appear to originate near graben on the flanks of Arsia Mons. Using new HRSC image data combined with MOLA, THEMIS and MOC data, we reexamine the smooth facies within and near graben on the flanks of Arsia Mons and assess in detail their origin and relation to the fan-shaped deposit as a whole. We consider several features high on the flanks of Arsia Mons that we interpret to be the most recent phase of



glaciation at Arsia. We also consider how these new data and this interpretation can provide broader insight into the nature and processes of glaciation, deglaciation and recent climate change on Mars.

## 2. Proximal Source Regions: Lineated Fill in the Large Graben

### 2.1. Description

[9] An  $\sim 8$ – $15$  km wide, 70 km long graben is present at an elevation of  $\sim 6$  km above Mars datum on the western flank of Arsia Mons (Figures 1–4). It comprises one segment of a much larger graben system that is generally oriented with long axes trending north–south (Figure 1). The graben may have originally formed due to regional extension [Montesi, 2001], late-stage volcanic activity (e.g., dike intrusion [e.g., Montesi, 2001; Wilson and Head, 2002a; Goudy and Schultz, 2005], explosive volcanism [e.g., Mouginis-Mark, 2002; Scott and Wilson, 2002], magma chamber evolution [e.g., Walter and Troll, 2001]), circumferential normal faulting due to central edifice loading [McGovern and Solomon, 1993], or loading on the lower flanks of the edifice [Montesi, 2001]. While this issue remains an open question, the general north–south trend of this graben system and comparisons with additional north–south trending graben systems within the fan-shaped deposit (Figure 1) [Zimbelman and Edgett, 1992] support a regional extension model for formation of the large graben. Regardless of the mechanism of formation, crater counting studies for the surface surrounding the graben give mid-to-late Amazonian age estimates [Scott and Zimbelman, 1995; Hartmann et al., 1999; Shean et al., 2006; Werner, 2006], suggesting relatively recent formation.

[10] A unique fill surface is present within the large graben that covers  $>1000$  km<sup>2</sup> and delineates the proximal margin of the Arsia fan-shaped deposit in these regions (Figure 1). The present depth of this graben ranges from  $\sim 0.3$ – $1.8$  km, measured from the top of the graben wall to the fill surface within the graben. The surface of the fill material in the graben is convex upward; latitudinal MOLA profiles show that it is highest in the center of the graben and lowest near the walls (Figure 5e), with at least  $\sim 250$  m of differential topography in places.

[11] The surface of the fill material within the graben is characterized by striking assemblages of arcuate ridges and furrows (Figure 3). Most of these ridges and furrows appear to represent variations in the surface of the fill material (Figure 3), in contrast to the distinctive depositional ridges of the ridged facies (interpreted to be drop moraines [Head

**Figure 3.** HRSC image data (12.5 m/pixel) showing the large graben (Orbit h1034). Note the prominent arcuate ridges and furrows on the surface of the graben fill. Two lobes can be identified (see Figure 4) by ridge patterns that are concentric to the alcoves along the southeastern graben wall. Also note the presence of surface ridge patterns near most walls of the graben. Three lobes of the graben fill are present to the west of the graben, two of which (lobes 1 and 2) appear continuous with the fill material (see Figure 4). Finally, note the depositional ridges to the east of the graben.

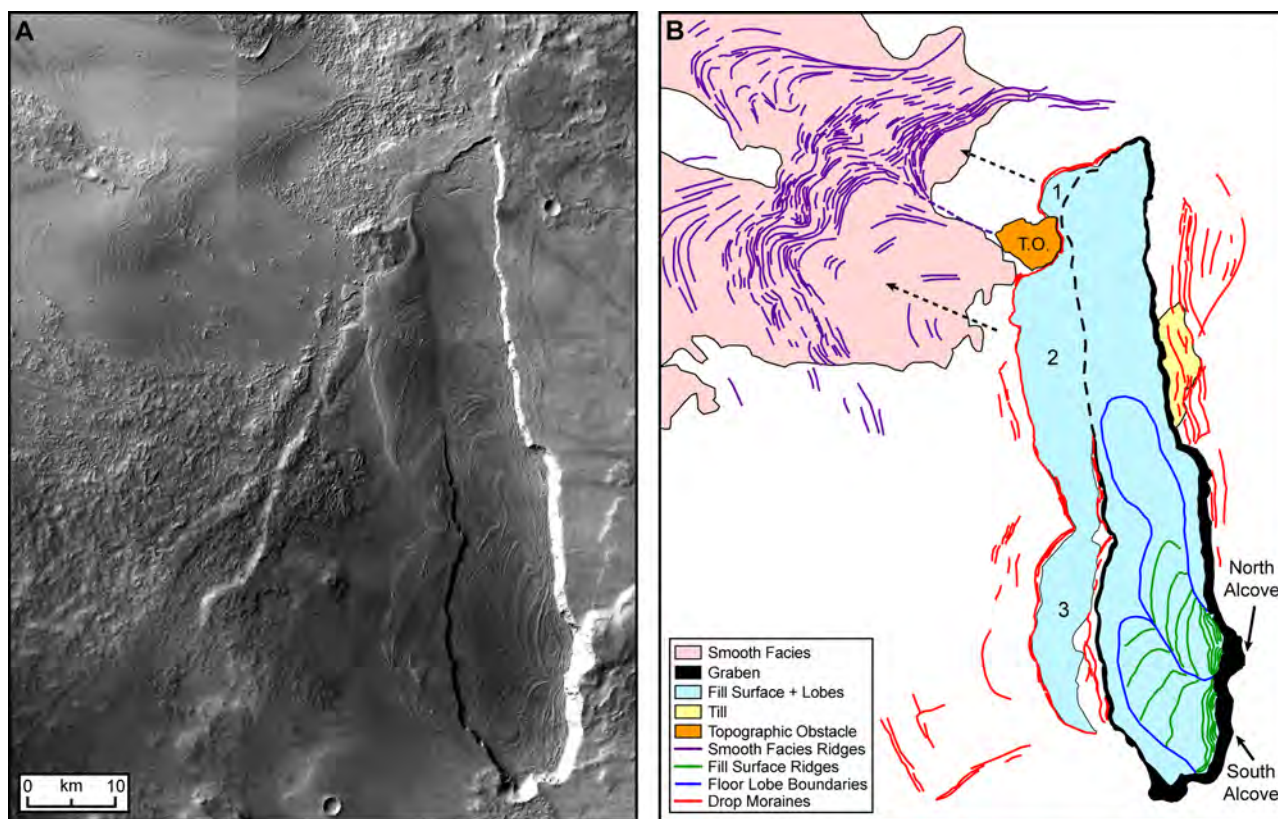


**Figure 4.** (a) HRSC image data of graben and proximal smooth facies lobes to the northwest (Orbits h1034 and h1045). (b) Sketch map of the region in Figure 4a. Graben fill and fill lobes west of the graben (labeled 1–3) are shaded light blue, with the interpreted position of the underlying graben wall as a dashed black line. The two primary glacial lobes on the floor of the graben are outlined with dark blue lines, and surface ridges that can be correlated between the two lobes are represented by green lines (refer to Figure 3 for more detail). Depositional ridges interpreted as drop moraines are represented as red lines. The smooth facies is mapped as light pink with the smooth facies ridges as purple lines. Note that the smooth facies ridges can be mapped beyond the present smooth facies boundary, suggesting that the smooth facies has experienced retreat since its formation. Note the concentric nature of the smooth facies ridges to the present boundaries of lobes 1 and 2. It appears that these proximal smooth facies lobes were sourced within the graben and represent an earlier phase of glacial activity. The dashed arrows indicate the apparent flow directions for the smooth facies lobes to the northwest around a  $\sim 400$  m relief topographic obstacle (labeled T.O. and shaded orange). See Figure 13 for additional detail of these features.

and Marchant, 2003; Head et al., manuscript in preparation, 2007]). They vary in both shape and size, with some peaked and others smoothed or rounded (Figures 3 and 4); most ridges appear to be a  $<10$  m high, while MOLA altimetric point data suggest that some attain heights of  $\sim 20$ – $30$  m above the surrounding fill surface (Figures 5a and 5e). The two most prominent assemblages (Figure 4) are concentric to adjacent alcoves along the base of the southeastern graben wall, where the greatest scarp relief is observed (Figures 3 and 5). The configuration of these ridge assemblages suggests northward flow of the material within the graben for at least  $\sim 30$  km (Figure 4). A close examination of individual ridges, ridge packets (closely spaced smaller ridges), and ridge spacing reveals that the same pattern is seen extending from both alcoves (Figure 4); at least nine ridges or ridge packets can be correlated between the two assemblages (green lines in Figure 4). The ridges from the northern alcove extend farther to the north, but both assemblages transition into fill material with no dominant orientation (Figures 3 and 4). Additional smaller assem-

blages of fill ridges are observed within a few kilometers of all graben walls (Figure 3). In the northern regions of the graben, the surface of the fill material often displays a rough texture or sets of aligned furrows, while in other locations, collections of blocks, boulders and debris can be observed on the fill surface (Figure 3).

[12] Along the northern half of the western wall, the fill material on the floor of the graben forms a continuous lobe over the  $\sim 200$ – $300$  m high graben wall that extends  $\sim 5$ – $10$  km downslope to the west (labeled as lobe 2, Figure 4). Surface ridges and lineations across this lobe are continuous with the fill material on the floor of the graben (Figure 3). Approximately halfway along the western wall of the graben, this lobe is separated from the fill material on the floor, exposing the underlying graben wall (Figure 3). This situation is also observed for the southern portions of the western wall where a  $\sim 1$ – $2$  km gap is observed between the wall of the graben and another distinct lobe of the fill material present on the surrounding surface to the west (lobe 3, Figures 3 and 4). MOLA profiles

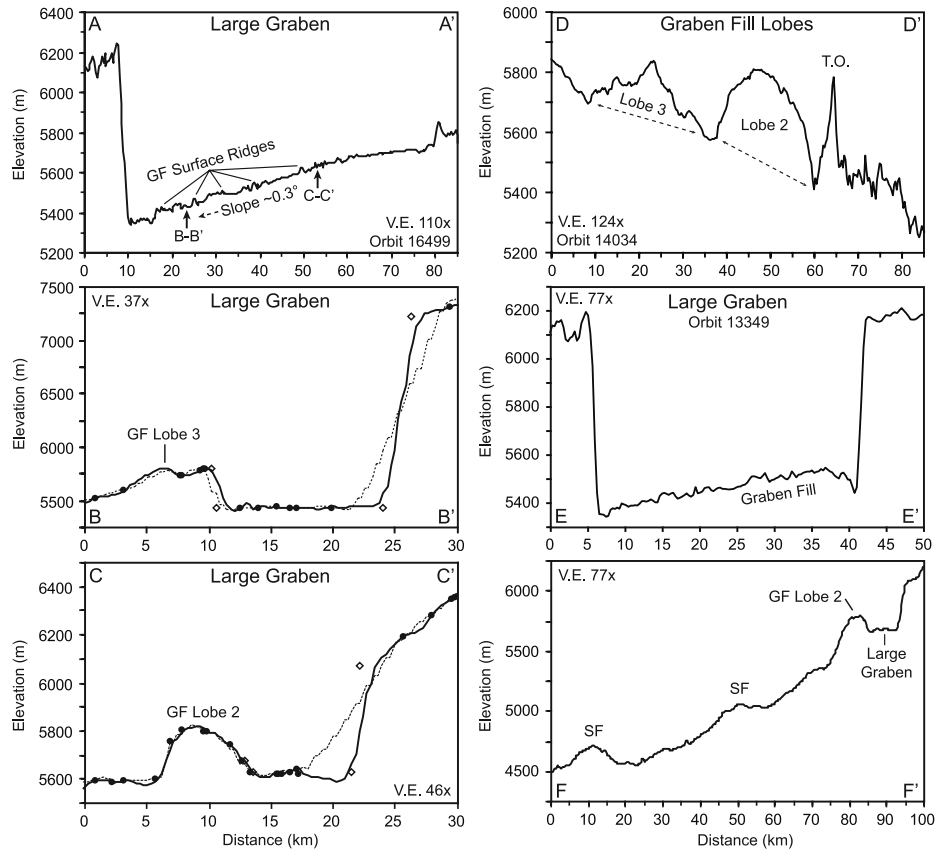


**Figure 5.** MOLA altimetry profiles for the large graben and surrounding areas. See Figure 2 for context. Profiles A-A', D-D', and E-E' were extracted from individual MOLA orbits with a point spacing of  $\sim 300$  m. The dashed line in profiles B-B' and C-C' was extracted from the MOLA 128 pixel/degree gridded data. The black circles show the locations of individual MOLA points that are within  $<150$  m of the extracted profile. The open diamonds represent the actual position of the top and bottom of the graben walls as measured on the HRSC image. The elevation assigned to these open diamonds was estimated by forecasting the slopes of surrounding MOLA points. The solid line in profiles B-B' and C-C' was extracted from a surface interpolated using the standard release, 200 m resolution HRSC DTM stretched over all available MOLA points in the vicinity of graben using an implicit interpolation algorithm. A comparison of the open diamonds with the MOLA grid and HRSC/MOLA interpolated surface profiles reveals that the MOLA gridded data are erroneous along the eastern wall of the graben due to large gaps between orbits (nearly a  $\sim 9$  km gap in these regions). The interpolated HRSC DTM/MOLA point surface provides a vast improvement over the MOLA gridded data for the eastern wall of the graben, providing a better fit for the actual graben wall. The two are similar where a higher density of MOLA points is available. This interpolated surface was only used for extraction of profiles B-B' and C-C'. Profile F-F' was extracted from MOLA 128 pixel/degree gridded data. (A-A') MOLA point data (orbit 16499) along the longitudinal (from south to north) axis of large graben. The solid arrows indicate the positions of profiles B-B' and C-C', which are normal to A-A'. Note the  $\sim 900$  m relief and steep slope of the southern wall in comparison to the  $\sim 150$  m relief of the northern wall. Also note the overall southerly trend of the fill material on the floor of the graben, with a slight break in slope near the C-C' crossing. The 300 m point spacing is able to resolve the larger surface ridges on the graben fill (labeled GF Surface Ridges), with some attaining heights of  $\sim 30$  m above the surrounding fill. (B-B') Profile crossing east-west over the deeper section of the graben. Note the high relief ( $>1800$  m) of the eastern graben wall along this profile and the depth relative to the western wall ( $>400$  m). Lobe 3 is also visible, although no MOLA points cross the lobe at this location. MOLA points (Orbit 14043) to the north show that Lobe 3 attains thicknesses of over  $\sim 150$  m. (C-C') Profile crossing east-west over the central regions of the graben. Note the relief of the eastern wall ( $\sim 500$  m) and the high relief of lobe 2 in these regions. (D-D') MOLA point data (orbit 14034) across the lobes of fill material and the topographic obstacle to the west of the graben. Note the high relief of the lobes ( $>200$  m) and the relative height of the topographic obstacle that splits lobes 1 and 2 (see Figure 4). (E-E') MOLA point data (orbit 13349) showing the convex nature of the fill within the graben. Note the  $>100$  m difference in topography between the central regions and near the walls of the graben. (F-F') Profile from the eastern graben wall, across lobe 2 and the proximal smooth facies lobes. Note the relief of the smooth facies lobes and their location downslope of the large graben.

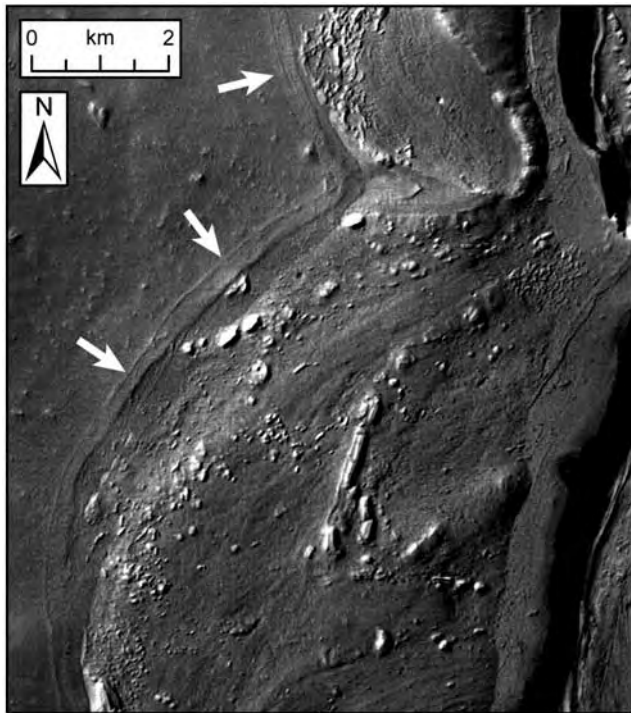


**Figure 6.** HRSC data (Orbit h1034) showing a close-up of the lobes of graben fill to the west of the graben. The junction between lobes 2 and 3 is observed in this figure (see Figure 4 for lobe definitions). White arrows point to the depositional ridges concentric to the margins of the lobes that are interpreted as drop moraines. Note the surface texture of the lobes, with large blocks and boulders and surface ridges like those observed to be continuous over the western wall between lobe 2 and the fill on the floor over the graben. Also note the separation and depositional features that are present between the eastern margin of the lobes and the western graben wall.

across these lobes reveal that they display local elevation differences of  $>250$  m in places, suggesting that the fill is at least  $\sim 250$  m thick in these locations (Figure 5).

[13] HRSC image data show additional ridges that are draped over the surfaces surrounding the graben (Figures 3, 4, and 6). However, unlike the ridges seen on the surface of the fill, these ridges appear to be depositional in nature and are present where the fill material is absent. These are most prominent to the east of the graben (red lines in Figure 4), at distances as far as  $\sim 11$  km from, and elevations of up to  $>300$  m above, the graben rim. They are generally concentric to the rim of the graben with some overlapping relationships observed (Figure 4). A collection of rough, hummocky material is present among a series of these depositional ridges beyond the eastern graben wall (Figure 3; yellow unit in Figure 4). Additional depositional ridges are observed around the margins of all three lobes to the west of the graben (red lines in Figure 4; Figure 6). These ridges are seen up to  $\sim 25$  km from the western graben wall and are generally concentric to the present margins of the lobes. At least two distinct, continuous ridges are observed immediately around the distal margins of all three lobes at distances of  $\sim 300$ – $700$  m (Figures 3, 4, and 6). Additional ridges are observed on the exposed surface between the proximal edge

of lobes 2 and 3, and the western graben wall (red lines in Figure 4; Figure 6).

## 2.2. Interpretation

[14] We considered several possible formation mechanisms for the features observed within and surrounding the large graben at Arsia Mons, including volcanic eruptions (i.e., pyroclastic deposit with the graben as a source vent) [Zimbelman and Edgett, 1992; Scott and Zimbelman, 1995], aufeis (groundwater-fed ice) [Garlick, 1988; Gillespie et al., 2005], rock glaciers [Lucchitta, 1981], and debris-covered glacier ice derived from atmospherically deposited snow and ice [Head and Marchant, 2003; Shean et al., 2005].

[15] The detailed morphology and topography of the graben fill argue against a pyroclastic origin. Although the two prominent lobes on the graben floor both originate along the southeastern graben wall, there is no evidence for specific vent-related structures at these locations. Furthermore, the lobes to the east of the graben (Figure 4) display topographic relationships that are significantly different from those typically associated with pyroclastic deposits [Shean et al., 2005], both on Earth [Cas and Wright, 1987] and Mars [Wilson and Head, 1994]. The shape and morphology of these lobes are also dissimilar from the vents and associated pyroclastic deposits seen on the flanks of the Tharsis Montes [Zimbelman and Edgett, 1992; Scott et al., 1998] and the more broadly vent-concentric phreatomagmatic eruptions elsewhere on Mars [Wilson and Head, 2004]. Finally, observations of the continuous fill draped over the western rim (lobe 2, Figure 4) and the  $>250$  m elevation difference between the fill on the floor and lobes to the east of the graben (Figure 5) are inconsistent with a pyroclastic interpretation.

[16] An interpretation as groundwater-fed glaciers (aufeis) also appears inconsistent with our observations. As identified by Head et al. [2005b], the general geothermal gradient in the Amazonian, the lack of surface meltwater features such as channels and gullies, and the lack of a significant recharge area or mechanism all argue against such an origin. In addition, there are several deep graben around Arsia Mons at much lower elevations than the large graben in question. Some of these graben are part of the same north/south trending system as the large graben, yet they display no evidence of the same ridged graben fill. If groundwater were responsible for fill generation, we would also expect the increased hydrologic head to produce similar deposits within these lower-elevation graben. Furthermore, the close association of the graben fill with the large Arsia Mons mountain glacier deposits argues for a related origin. If the features within the graben represent aufeis processes, this would require that the groundwater-fed aufeis produced an ice sheet extending  $>450$  km from the graben, with a volume of  $\sim 3$ – $4 \times 10^5$  km<sup>3</sup> (covering an area of  $\sim 166,000$  km<sup>2</sup>). This represents a highly unlikely scenario considering the expected rapid refreezing of groundwater in the near subsurface, even in the vicinity of dikes [Head and Wilson, 2002; Wilson and Head, 2002b].

[17] There is much discussion in the terrestrial literature regarding the definitions and distinguishing characteristics of features often referred to as rock glaciers. These features flow by creep deformation of internal ice and

often display a characteristic ridge and furrow surface morphology. We define rock glaciers as features that primarily consist of debris with interstitial ice of secondary origin [e.g., *Wahrhaftig and Cox, 1959; White, 1976; Hassinger and Mayewski, 1983; Barsch, 1996*] and distinguish debris-covered glaciers as features that have a demonstrable core of glacier ice covered by a thin (cm to m scale) layer of surface debris. This debris layer may develop from rockfall, atmospheric dust/ash deposition, and/or ice loss in the ablation zone to produce a lag deposit [e.g., *Potter, 1972; Ackert, 1998; Potter et al., 1998; Konrad et al., 1999; Rignot et al., 2002*]. It is important to note that despite nearly 100 years work, terrestrial researchers have not yet reached a consensus on the proper nomenclature and classification schemes to use when describing these features. While many would agree that rock glaciers and debris-covered glaciers are genetically distinct, others suggest that they represent different stages of rock glacier development and/or end-members of a continuum. Excellent reviews of these issues are given by *Whalley and Martin [1992], Whalley and Azizi [1994, 2003], and Hamilton and Whalley [1995]*.

[18] In the Arsia examples, the long flow distances (>30 km), the continuous relationship between the fill on the floor and the lobes west of the rim (Figure 3), and the magnitude of implied volatile loss from the topographic difference between the current rim and the floor all suggest that these features do not represent rock glaciers with high debris/ice ratios. Many of the arguments against the rock glacier, pyroclastic flow and aufeis hypotheses also apply to landslide or gravity-driven mass-wasting hypotheses for the graben fill (see further discussions by *Head and Marchant [2003]* and *Shean et al. [2005]*).

[19] After detailed review of new observations, we interpret the fill material on the floor of the large graben at Arsia Mons to be waning stages of debris-covered glaciers that filled the graben in the past. The collections of ridges and furrows on the fill surface suggest that the two alcoves on the southeastern wall of the graben served as the accumulation areas for two large debris-covered glaciers that were the primary source of ice within the graben (Figures 3 and 4). Corresponding patterns of ridges and ridge packets on each of these glaciers (Figure 4) suggest that they formed simultaneously in the two cirque-like alcoves, with the same atmospheric source, and flowed northward along the long axis of the graben.

[20] We interpret the ridges on the surfaces around the rim of the graben (Figures 4 and 6) to be drop moraines deposited by the debris-covered ice during stages of retreat. Their distribution is concentric to the graben walls and lobe margins, suggesting that the fill material covered a larger area in the past. Although the fill surface currently lies ~0.2–1.8 km below the graben rim, the moraines and continuous lobes (lobes 1 and 2, Figure 4) over the northwestern graben wall indicate that at one time, debris-covered ice completely filled the graben, breached the walls, and extended an additional ~5–11 km to the east, and at least 25 km west of the graben. After reaching this larger extent, we suggest that subsequent ice retreat resulted in moraine deposition, thinning, and the eventual severance of lobe 3 from the fill within the graben, exposing the underlying graben wall. However, the observation that the

fill material appears to be >250 m thick in places (Figure 5) suggests that a significant volume of ice may still remain beneath the debris cover on the western lobes and possibly on the floor of the graben.

### 2.3. Implications for Climate Change on Mars

[21] Specific glacial and periglacial features (e.g., layering in ice, moraine sequences, till stratigraphy, etc.) can record important information related to temporal aspects of climate change both on the Earth [e.g., *Bickerton and Matthews, 1993; Marchant et al., 1994; Gosse et al., 1995*] and Mars [e.g., *Laskar et al., 2002, 2004; Head et al., 2003; Perron et al., 2003b; Milkovich and Head, 2005*]. Within the large graben, the relative spacing between corresponding ridges on the two debris-covered glaciers is greater for the glacier extending from the southern alcove, suggesting faster flow or less compression than the glacier extending from the northern alcove (Figure 4). Regardless of the reasons for the disparity in spacing between these ridges and ridge packets, it is clear that the ridges themselves represent a signal. We interpret the data to indicate that these glaciers were formed due to atmospheric precipitation, collection and preservation of snow within the alcoves, which underwent compaction to form glacial ice that eventually flowed northward and filled the graben. The similar patterns of ridges on the two lobes extending from the large alcoves along the southeastern graben wall (Figure 4) suggest that a common process is responsible for surface ridge formation. The signal contained within the ridges is undoubtedly complex, with many potential factors contributing to ridge size and spacing (i.e., periods of increased snow accumulation or debris inclusion, warmer temperatures resulting in faster ice flow/compression, etc.).

[22] This fill surface ridge signal is not unlike the climate signal contained within the ~150 ridges of the outer ridged facies of the Arsia Mons fan-shaped deposit (*Head et al., manuscript in preparation, 2007*). The spacing and size of the ridged facies is variable, with closely spaced ridge packets also observed. However, the ridged facies was deposited earlier in the Late Amazonian [*Shean et al., 2006; Head et al., manuscript in preparation, 2007*]. The significance of the ridge structure within the graben and the ridged facies on the distal flank of Arsia is that they may potentially provide clues to understand the climate record for periods in Mars history when equatorial ice accumulation occurred [e.g., *Forget et al., 2006; Shean et al., 2006*]. Understanding the precise conditions necessary for this type of glaciation is under investigation, but they are believed to be related to extended periods of higher mean obliquity [*Head and Marchant, 2003; Haberle et al., 2004; Head et al., 2005a; Shean et al., 2005; Forget et al., 2006; Head et al., manuscript in preparation, 2007*]. The variation responsible for production of the individual ridges on the surface of the graben fill may be driven by the 120,000-year obliquity cycles during these periods of higher mean obliquity [*Shean et al., 2006; Head et al., manuscript in preparation, 2007*], but at this time it is difficult to rule out other possible cycles and/or causes.

### 2.4. Candidate Debris Sources and Implications

[23] The morphology of the areally extensive and relatively thick Tharsis Montes fan-shaped deposits suggests

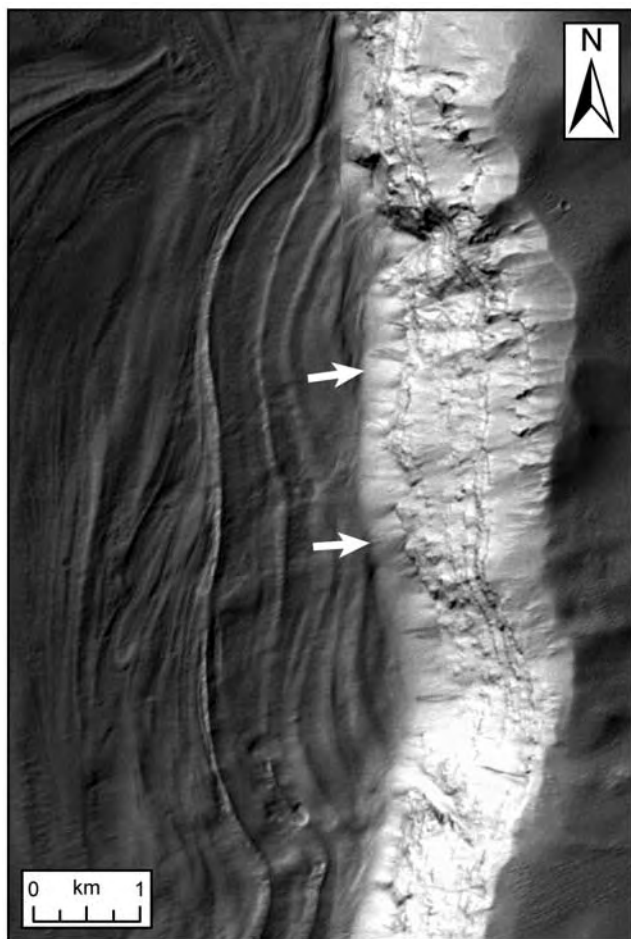


**Figure 7.** HRSC data (Orbit h1034) showing a close-up of the southern alcove (see Figure 2 for context). White arrows point to the series of debris aprons that extend from the base of graben walls onto the surface of the fill material. Note the concentric nature of the five distinct fill surface ridges within  $\sim 1$  km of the alcove. The relief of the eastern graben wall is  $\sim 1$  km in these regions.

that they are composed mostly of debris deposited during retreat and deglaciation [Head and Marchant, 2003; Shean et al., 2005; Head et al., manuscript in preparation, 2007]. However, one of the key questions in their interpretation is the source of this debris. The interpreted cold-based nature of the glaciation responsible for producing the deposits implies that basal scour and incorporation of subglacial debris were very minimal or nonexistent [e.g., Benn and Evans, 1998; Cuffey et al., 2000; Atkins et al., 2002; Head and Marchant, 2003]. Instead, three contributing sources have been suggested for the debris that produced the fan-shaped deposits [Head and Marchant, 2003; Shean et al., 2005]: (1) airfall of atmospheric dust, either as condensation nuclei for snow, or simply settling out of the atmosphere, (2) airfall of pyroclastic ash from plinian volcanic eruptions [e.g., Mouginis-Mark, 2002], and (3) rockfall from cliffs and scarps above the glacier and near accumulation zones. The remarkable homogeneity and regular distribution of the ridged and knobby facies suggest that the debris was well distributed over the glaciers, with

atmospheric deposition of dust and/or volcanic ash as the most likely source(s) [Lucchitta, 1981; Head and Marchant, 2003; Shean et al., 2005].

[24] The high relief and steep slopes of the graben walls contribute a third potential source for debris, as localized rockfall in the accumulation zone(s) of these glaciers. HRSC data clearly show talus cones, debris fans and slope streaks extending onto the fill surface near walls of the graben, especially within the two alcoves believed to be primary accumulation areas for the glaciers within the graben (Figures 4 and 7). Also note (Figure 3) that the source regions (North Alcove and South Alcove) for the two main lobes on the floor of the graben appear “indented” relative to the remainder of eastern graben wall, an observation that is consistent with backwasting and scarp retreat, which would result in rockfall. This is supported by observations of terrestrial debris-covered glaciers where rockfall in accumulation zones is the primary debris cover source [Potter, 1972; Ackert, 1998; Benn and Evans, 1998]. Thus, on the basis of terrestrial analogs and our observations of the present debris fans and talus cones, we suggest that debris falling from the graben walls was the primary source for debris cover formation on the glaciers within the large Arsia graben.

[25] It is interesting to consider the amount of material that could be derived through rockfall from the graben walls. The eastern and western walls of the graben are not linear – the southern half of the graben is wider and the eastern wall appears to be  $\sim 2$  km farther to the east than a linear extension of the northern half of the eastern wall would suggest (Figure 3). If the original graben was more symmetrical and achieved its present widened configuration through scarp retreat, then a significant portion of this material would be available for glacial debris cover formation. Estimates of typical scarp retreat rates on Mars are poorly constrained, but considering the Mid-to-Late-Amazonian age of units cut by the graben [Scott and Zimbelman, 1995], it is not unreasonable to assume that a significant portion of this retreat could have occurred when these glaciers were forming. If we assume that the entire  $\sim 2$  km width increase was the result of eastward scarp retreat, and assume an average graben depth of  $\sim 1$  km along this  $\sim 35$  km section of the scarp, then it is possible that a volume of  $\sim 70$  km<sup>3</sup> was removed. This volume of material would be sufficient to cover the  $\sim 1000$  km<sup>2</sup> graben fill surface with  $\sim 70$  m of debris or the entire  $\sim 166,000$  km<sup>2</sup> deposit at Arsia Mons with  $\sim 0.4$  m of debris. While it is unlikely that the debris from this small section of the graben could be evenly distributed over the entire Arsia deposit, it is important to consider the potential contribution of rockfall as a debris cover for glacial deposits near scarps that also serve as glacier accumulation areas on Mars. However, as will be discussed later, a relationship between the graben fill and the larger smooth facies lobes suggests that rockfall debris within the graben could easily be spread over a significant part of the larger Arsia mountain glacier.

### 3. Terrestrial Analogs

[26] The hyperarid, polar desert climate of the Antarctic Dry Valleys provides one of the best terrestrial analogs for many geologic processes on Mars [e.g., Mahaney et

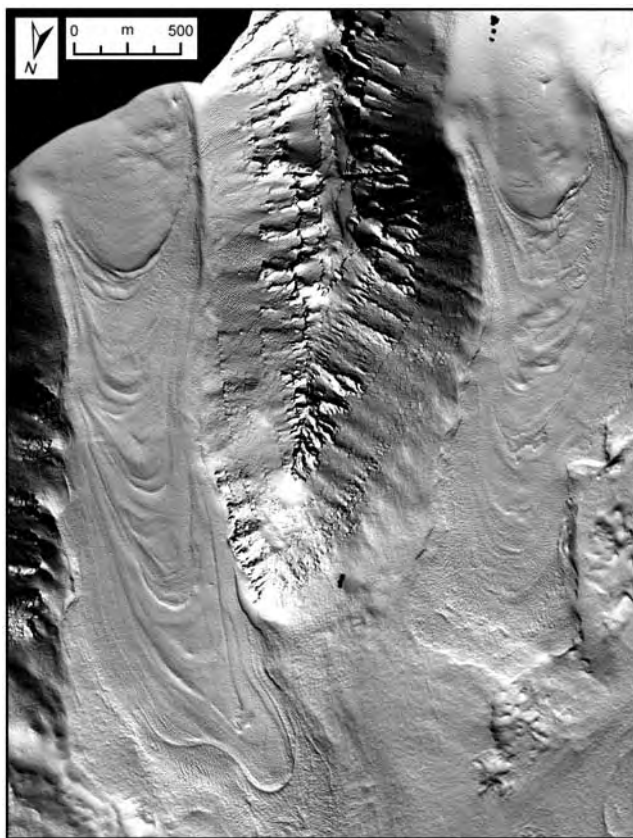


**Figure 8.** Shaded relief map from 2 m resolution LIDAR topography of Upper Beacon Valley, Antarctica showing debris-covered glaciers in Mullins Valley (left) and Friedman Valley (right). Note the well-developed ridge and furrow patterns on the surface of both glaciers. The ridges represent actual variations in the ice surface beneath a uniform layer of debris.

*al.*, 2001; *Arcone et al.*, 2002; *MacClune et al.*, 2003; *Wentworth et al.*, 2005]. The tributaries of upper Beacon Valley (Figure 8) are occupied by debris-covered glaciers [*Rignot et al.*, 2002; *Lorrey*, 2005; *Levy et al.*, 2006; *Shean et al.*, 2007] that provide excellent analogs for the features within the graben at Arsia Mons. The debris-covered glacier that occupies one of these tributaries, Mullins Valley, is ~6–8 km long, ~1 km wide, and consists of a relatively pure, ~40–95 m thick glacier ice core as revealed by shallow seismic reflection surveys [*Shean et al.*, 2007]. The surface of this glacier is characterized by ~1–5 m high, arcuate ridges and furrows (Figure 8) with a continuous debris cover in the ablation zone that ranges from ~0.1–1.0 m [*Lorrey*, 2002]. The source of this debris cover is predominantly rockfall from the surrounding dolerite and sandstone cliffs near the accumulation zone of the glacier. As the ice flows downvalley, the thickness of the debris cover increases due to sublimation of debris-containing ice in the relatively extensive ablation zone of the glacier [*Ackert*, 1998; *Lorrey*, 2002]. Eventually, this thickening debris cover enhances preservation of the underlying ice [*Nakawo and Young*, 1982; *Bozhinskiy et al.*, 1986; *Nakawo and Rana*, 1999], contributing to reduce sublimation to

insignificant rates [*Marchant et al.*, 2002; *Kowalewski et al.*, 2006] compared to annual accumulation.

[27] A similar pattern of ridges and furrows is observed on the surface of the debris-covered glacier occupying Friedman Valley, another tributary of Beacon Valley that is adjacent to Mullins (Figure 8). It appears that in the past, these two glaciers may have formed and interacted in a similar manner to the two debris-covered glaciers originating at the alcoves within the Arsia graben. Preliminary work suggests that at least four of the large surface ridges on the glaciers in Mullins and Friedman Valley can be matched using aerial photos and topography data. Unfortunately, the mechanism of formation for the surface ridges is poorly understood for terrestrial glaciers, so any extrapolation to Mars is difficult. The present literature suggests that surface ridge and furrow patterns may be related to external factors (e.g., debris input, climate changes that affect mass balance or ice velocity), internal factors (e.g., internal structure, thrusting or folding within the ice), or some combination of these factors [*Loewenherz et al.*, 1989; *Kaab and Weber*, 2004]. On the basis of age estimates and measured flow rates for the glaciers within Mullins and Friedman Valley, we suggest that the surface ridges could be forming due to orbitally driven glacial cycles influencing external factors (temperature increases, ice velocity increases, accumulation increases, etc.) [*Shean et al.*, 2007]. During the warmer interglacials, we might expect increased ice flux, leading to compression and thrusting within the ice to form the surface ridges [*Shean et al.*, 2007].

#### 4. Evidence for Additional High-Elevation Glacial Features at Arsia Mons

[28] In addition to the large graben, several other depressions at high elevations on the flanks of Arsia Mons display evidence for glacial activity (Figures 1 and 2). We briefly describe these features and assess their similarities and differences, relative to the large graben. We also discuss the implications of these new observations and how they can help to improve our understanding of the conditions necessary for localized ice accumulation, the formation of the smooth facies, and the formation of the Arsia Mons mountain glacial deposits as a whole.

##### 4.1. Debris-Covered Glacier in the Northern Graben

[29] The large graben on the flanks of Arsia Mons is only one segment within a series of large extensional features characterized by approximately north–south to northwest–southeast orientation (Figures 1 and 2). Another large segment of this graben, situated to the northwest of the large graben (Figure 2), is filled with smooth facies material at lower elevations (Figure 1). HRSC data reveals that at the highest elevations within this graben, a distinctive lobate feature is observed (Figure 9) that does not have a “deflated” appearance like many flow-like features on Mars. It is ~10 km long, 2–4 km wide and ~100 m thick (Figure 9). In plan view, it appears lobate with a larger head and thinner neck that does not completely fill the graben, leaving ~1–1.5 km between the graben walls and the lateral margins of the neck (Figure 9). The northern portion of the wider lobate section is characterized by a series of concentric ridges (Figure 9) similar to those observed on

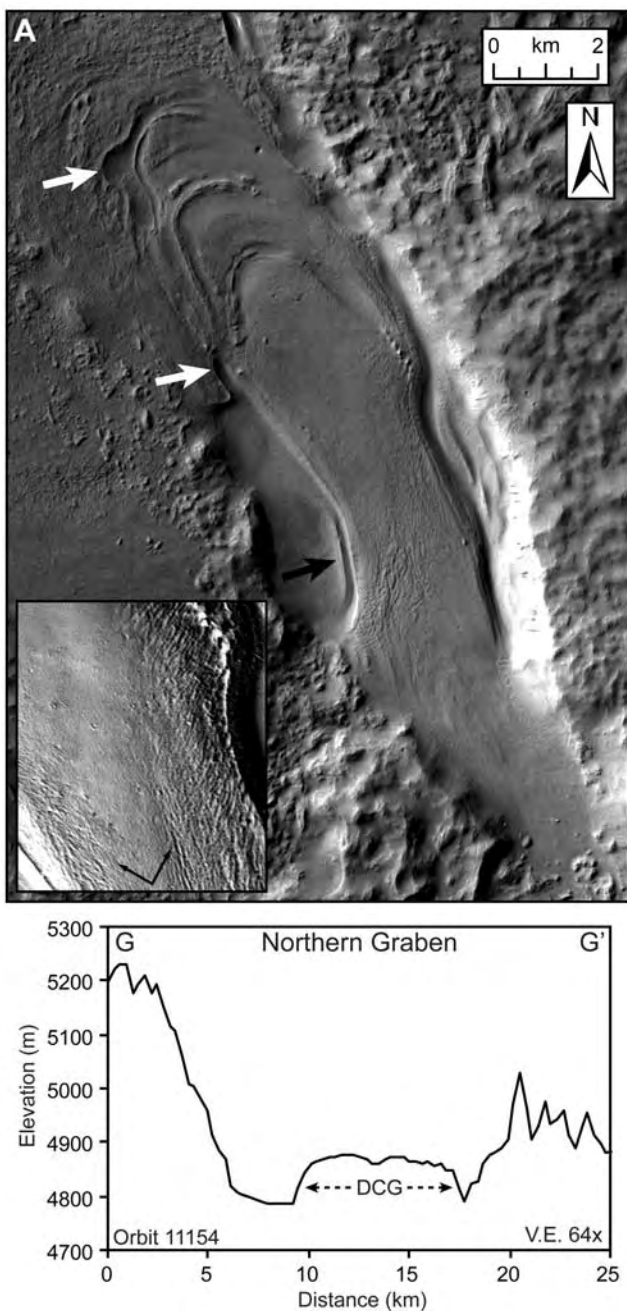


**Figure 9.** (a) HRSC data (Orbit h1034) showing the lobate feature interpreted as a debris-covered glacier in the northern graben (see Figure 2 for context). Note the arcuate ridge and furrow patterns on the surface in the thicker distal regions, the ridges with inward depressions (white arrows) suggesting retreat and ice loss, and lateral ridges (black arrow) along the thinner neck. Inset MOC image (E1001872) shows chevron-like structures on the surface of the lobe. These features are oriented at an angle to the margins of the lobe as indicated by the thin, solid arrows. (G-G') MOLA point data (Orbit 1154) across the lobate feature (labeled DCG) in the northern graben. This profile shows that interpreted debris-covered glacier attains thicknesses of  $\sim 80$ – $90$  m above the floor of the northern graben (see Figure 2 for profile context).

the fill surface within the large Arsia graben (Figure 3). In addition to the space between the graben walls and the thinner neck, marginal ridges and depressions suggest previous occupation of a larger portion of the graben by the lobate feature (white arrows in Figure 9). These ridges with inward depressions are similar to moraine-like ridges commonly observed on crater floors at the base of gullied walls [Howard, 2003; Milliken *et al.*, 2003; Marchant and Head, 2003; Arfstrom and Hartmann, 2005]. Finally, MOC image data of the lobe reveal a rough surface with chevron-like lineations oriented at approximately  $45^\circ$  to the margins (inset, Figure 9). These features appear to be structural and not simply dunes or oriented debris on the surface of the lobate feature. Instead, they are similar to chevron crevasse patterns that are observed on some terrestrial glaciers bounded by valley walls. These chevron crevasses are opened by tensile stresses that arise from faster ice velocities along the center of the glacier and drag along the valley walls [Benn and Evans, 1998].

[30] On the basis of these characteristics we interpret this flow-like feature in the northern graben to be a debris-covered glacier. Cross-sectional profiles (Figure 9) suggest that it may still contain a significant ice core,  $>100$  m thick in places. In addition, the marginal depressions and lateral ridges suggest that this feature has experienced some retreat.

#### 4.2. Moraines and Till Downslope of Smaller Graben

[31] Another smaller graben ( $\sim 18$  km long,  $\sim 3$ – $4$  km wide,  $>1$  km deep, Figure 10) is observed  $\sim 50$  km to the south of the large graben (Figures 1 and 2) at approximately the same elevation (Figure 10). This graben also contains fill material on its floor (Figure 10), and although it appears highly dissected when compared to the fill on the floor of the large graben (Figure 3), it displays similar arcuate, fill surface ridges and furrows around the western wall of the graben. As was observed within the larger graben, a continuous series of debris fans and slope streaks are present along the graben walls extending onto the fill surface. However, unlike the fill material in the larger Arsia graben, a convex topographic signature is not observed.

[32] Following local westerly slopes down the Arsia Mons flank, a total of 25 depositional ridges are present extending out to distances of  $>60$  km from the western graben wall (gray lines in Figure 10; white arrows in Figure 11). These depositional ridges are concentric to the western wall of the graben, with some of the most proximal ridges displaying the same shape as individual alcoves in the western graben wall (Figure 10). Many of these ridges are draped over the underlying topography and some appear perched on the sides of large hills that are  $>200$  m high (Figures 10 and 11c). A few additional ridges are present to the east of the graben as well (Figure 10), similar to those observed to the east of the large Arsia graben (Figures 3 and 4). On the basis of their similarity to drop moraines in the Antarctic Dry Valleys observed within Arena Valley [Brook *et al.*, 1993], the Olympus Range [Vanden Heuvel, 2002], and the Wilkness Mountains [Staiger *et al.*, 2006], as well as to those in ridged facies of the distal portions of the Arsia Mons deposit and surrounding the lobes of the Arsia graben fill, these ridges are also interpreted as drop moraines.

[33] These ridges bound a distinctive, homogeneous assemblage of knobs and debris that comprise a well-

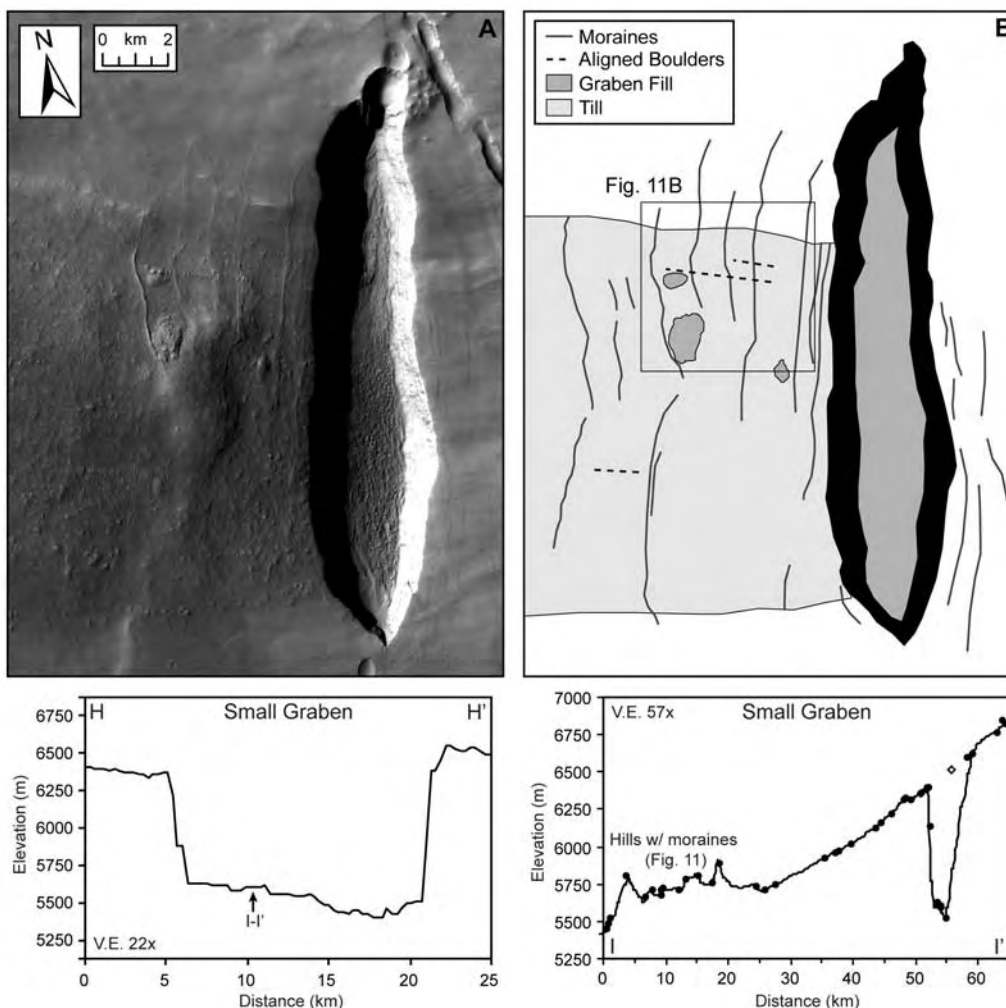


**Figure 10.** (a) HRSC data (Orbit h1034) of the smaller graben. Note the dissected fill texture on the floor and the fill surface ridges near the edge of the shadow from the western wall (these are also visible using a different stretch within the shadowed region). (b) Sketch map for area in Figure 10a. Note the depositional ridges (solid gray lines) that are concentric to the graben walls both to the east (upslope) and west (downslope) of the graben; these are interpreted as drop moraines. Note the lower-albedo band of debris (light gray unit), with aligned boulders (dashed lines) that is bound to the north and south by these moraines. This hummocky unit is interpreted as a glacial till. Also note the patches of debris-covered fill (dark gray) located between a prominent moraine and a topographic high. Additional patches of similar material are present  $\sim 40$  km to the west between another prominent moraine and hills (see Figure 11). This material is interpreted as remnant debris-covered ice from the glacier that produced the drop moraines and till west of the small graben. The solid black box shows the location for a zoomed view of the moraines, aligned boulders and debris-covered fill (Figure 11b). (H-H') Longitudinal profile extracted from MOLA 128 pixel/degree gridded data across the small graben. Note the  $\sim 1$  km relief of the graben and the general northward slope of the dissected graben fill. The solid arrow indicates the position of profile I-I', which is normal to G-G'. (I-I') Profile extracted from MOLA 128 pixel/degree gridded data that crosses the small graben and the hills to the west, where perched moraines, till, and remnant fill are observed (see Figure 11). As described in Figure 5, the open diamond indicates the location of the eastern graben wall from HRSC image data with forecasted elevation from MOLA points. Note the relatively large depth/diameter ratio of the graben, the difference in elevation of the eastern and western walls, and the relief of the hills to the west of the smaller graben.

defined band to the west of the smaller graben (Figure 1; light gray unit in Figure 10). This area has a slightly lower albedo than the surrounding terrain and collections of boulders aligned perpendicular to the long axis of the graben and ridges are also observed (dashed lines in

Figure 10; Figure 11c). On the basis of these observations, we interpret this deposit to be a till deposited during retreat of the glacial ice that also formed the moraines.

[34] In addition to the features interpreted as moraines and till downslope of the smaller graben, isolated patches of what

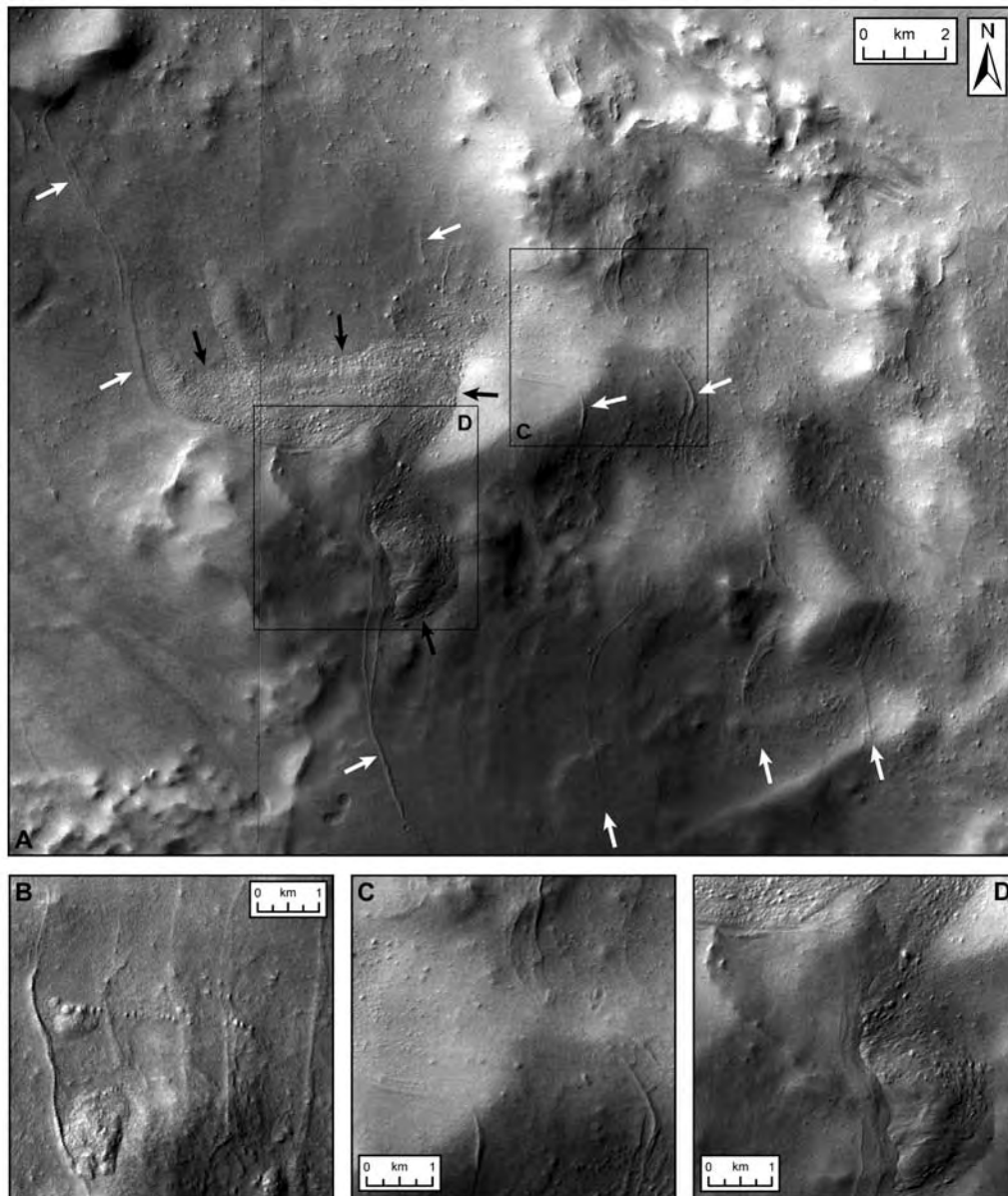


**Figure 11.** (a) HRSC data (Orbits h1034 and h1045) showing extensive depositional ridges, debris, and remnant fill material among hills  $\sim 35\text{--}55$  km west of the small graben. Solid white arrows indicate some of the depositional ridges interpreted as drop moraines. Solid black arrows outline margin of remnant fill material that is present to the east of a prominent moraine and is confined to the sides of hills. (b) Section to the west of the smaller graben showing moraines, aligned boulders, and debris-covered fill material between the prominent moraine on the left side of the image and the local topography. See Figure 10 for context. (c) Section of region in Figure 11a showing perched ridges interpreted as drop moraines. Note how some of these features are perched on the sides of hills that display  $>200$  m of relief (Figure 10). (d) Section of region in Figure 11a showing debris-covered fill and bounding moraines. This material is interpreted as remnant debris-covered glacial ice on the basis of its context, convex upward topography, and rough, debris-covered surface.

appears to be debris-covered fill material are observed on the same surfaces. The first patch is present  $\sim 4$  km from the western graben wall on the western side of a topographic obstacle (dark gray unit in Figure 10; Figure 11b). The surface of this material is convex upward and appears rough, distinguishing it from the surrounding material. Both this particular patch and another small patch immediately to the north (Figures 10 and 11b) are situated on the proximal side

of a very prominent moraine (Figures 10 and 11b). A more distinctive patch of this same material is observed  $\sim 45$  km to the west of the graben (solid black arrows in Figure 11). The fill is concentrated on the proximal side of another prominent moraine that stretches across large hills (Figure 11d). It covers a larger area ( $\sim 23$  km<sup>2</sup>) than the patches near the smaller graben and appears continuous between two hills that are  $>200$  m high (Figures 10 and 11). The surface of this

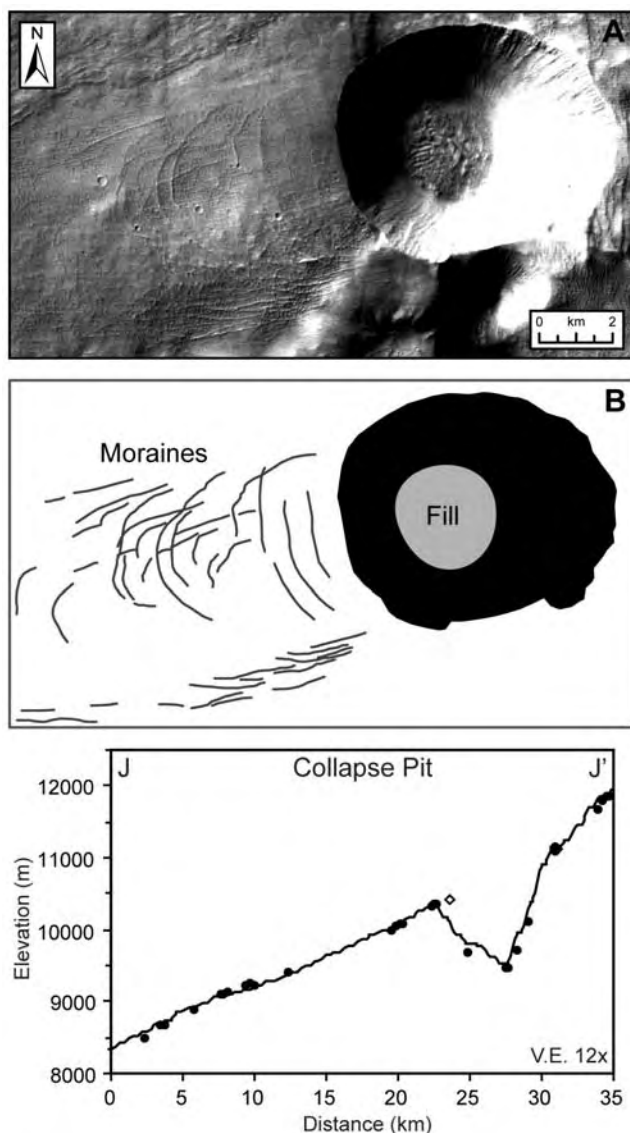


**Figure 12.** (a) HRSC data (Orbit h1023 with 1024-pixel high pass filter) of a large collapse pit high on western flank of Arsia Mons. Note the presence of what appears to be dissected fill on the floor of the pit (shaded gray). (b) Sketch map of the region in Figure 12a. Note the arcuate, concentric ridges present to the west of the collapse pit (solid gray lines). These ridges are observed up to 24 km from the eastern wall of the collapse pit, display cross-cutting relationships, and are interpreted as drop moraines. Also note the presence of polygonal dunes within the region bounded by the drop moraines. (J-J') Profile extracted from MOLA 128 pixel/degree gridded data across the large collapse pit. Note the high relief and relative elevations of the eastern and western walls. Vertical exaggeration of this profile is also much smaller than other profiles.

patch is smooth in some areas, but is mostly covered by debris and large boulders, making it easily distinguishable from the surrounding terrain (Figure 11).

[35] We interpret these observations as evidence that a glacier, with its source at the eastern graben wall, filled the graben and flowed down local slopes to the west for >60 km.

As it retreated, this glacier deposited drop moraines and till, with some isolated patches of debris-covered ice preserved near obstacles.

#### 4.3. Moraines Downslope of a Large Collapse Pit

[36] Additional evidence for high-elevation glaciation is observed ~80 km to the southeast of the smaller graben discussed in the previous section, near a collapse pit high on the flanks of the Arsia shield at an elevation of ~10.5 km above Mars datum (Figures 1 and 2). The pit has a diameter of ~6–7 km and a depth of ~1 km (Figure 12) and represents the largest segment of a linear collection of collapse features (Figure 2). HRSC data show that like the other high-elevation graben on the western flanks of Arsia, it also contains dissected fill material on its floor (Figure 12). This observation distinguishes this large collapse pit from hundreds of smaller circular collapse features on the southern and northern flank of Arsia Mons, which typically have smooth floors and no evidence of this dissected fill material [Dickson *et al.*, 2005].

[37] To the west of the pit are a series of arcuate ridges that extend nearly 24 km from the western wall down local slopes (Figure 12). Detailed mapping reveals that these ridges display cross-cutting and superposition relationships in a few places (Figure 12). In addition, numerous dunes with polygonal patterns are observed near the pit, primarily within the area bounded by the ridges (Figure 12).

[38] We interpret these features as drop moraines deposited by a relatively small cold-based glacial lobe that had its source at the collapse pit. These features and their overlapping relationships are similar to depositional ridges recently observed within a large crater at 70°N that were also interpreted as drop moraines deposited by a small glacier on the rim and within the crater [Garvin *et al.*, 2006].

#### 4.4. Common Characteristics and Similarities of High-Elevation Features

[39] On the basis of the distinctive structures and textures (e.g., fill surface ridges, concentric depositional ridges, etc.) associated with these depressions located high on the western flank of Arsia Mons, we interpret these locations as sites of past glacial activity. By considering all of these features and their similarities, we can better understand the conditions necessary for this type of localized glaciation, as well as the conditions that might produce the larger scale mountain glaciers at the Tharsis Montes.

[40] The features within the graben all occur at ~6.0–7.0 km elevation on the western flanks of Arsia Mons. As previously mentioned, there are additional graben of similar dimensions at lower elevations at Arsia that do not display the same evidence for glacial activity. This suggests that the high elevation of these features may be an important factor for the initiation of these glacial processes. Another similarity shared by all four of these distinctive features associated with glacial activity is the relative elevations and relief of their eastern vs. western slopes (Figures 5, 10, and 12). In each case, the eastern wall is present at significantly higher elevations and displays greater relief than the western wall. This is not surprising, considering the local westward slopes of the surface of the Arsia edifice (~3.5–5.5°) before the collapse features were formed. These relationships suggest that each of these depressions (except for the

northern graben) was filled with snow and ice that eventually overflowed the lower western wall and experienced additional downslope flow to the west. Although the terrain above the eastern wall could have provided an additional accumulation area [e.g., *Rea et al.*, 1999], the higher eastern wall appears to have served as the primary location for snow collection, maintaining an accumulation area within the graben to feed the glacier flowing over the lower western wall. In addition, the high eastern wall would continue to provide a source of debris from rockfall, which would result in much more prominent glacial deposits such as moraines or till, and eventually a thicker, more continuous debris cover allowing for extended preservation. The significance of the high eastern wall for the large graben is readily apparent in Figure 1b, which shows the crucial location of the large graben at a major break in regional slope near the base of the main edifice. A moist air mass traveling upslope and cooling adiabatically might deposit a significant amount of snowfall [e.g., *Forget et al.*, 2006] upon encountering the abrupt elevation increase of the eastern graben wall. In addition to direct atmospheric precipitation, we might also expect windblown snow or frost in the region to preferentially collect within these depressions.

[41] It is interesting to note that several adjacent west-facing scarps with similar relief exist within the same elevation range on the western flank of Arsia (see black arrow, Figure 2). If the requirements for this glacial activity were simply a large scarp to serve as an accumulation area and to provide sufficient debris for debris-cover formation, then we would expect to see similar features (e.g., remnant fill, moraines, till, aligned boulders, etc.) extending downslope from these scarps; however, no glacial deposits are observed at these locations. This suggests that the presence of a depression in addition to a high-relief, west-facing scarp are required for this style of high-elevation glacial activity. In addition to enhanced accumulation (via direct atmospheric precipitation and windblown snow collection), the unique insolation environment within these deep depressions could allow for enhanced preservation of snow and ice on the floor. These insolation variations have been considered for circum-polar craters at high latitudes on Mars [*Russell et al.*, 2003; *Russell and Head*, 2005], where they are believed to be responsible for the unique topography and preservation of volatile-rich deposits in crater centers [*Garvin et al.*, 2000; *Russell and Head*, 2005; *Kreslavsky et al.*, 2007]. In addition to insolation, the temperature-pressure conditions or local wind environments at the base of a  $\sim 1$  km deep graben might enhance ice preservation. The importance of topographic basins for glacial initiation and preservation has been documented for terrestrial glaciers in Patagonia [*Hulton and Sugden*, 1997] and Scotland [*Payne and Sugden*, 1990].

## 5. Age Estimates

[42] Using HRSC image data, all craters larger than  $\sim 50$  m in diameter were catalogued for the  $>1000$  m<sup>2</sup> fill surface within the graben and the three lobes to the west of the graben wall. The results of this effort reveal that a total of 7 craters fall within the 250 m bin using the *Hartmann* [2005] crater counting methodology. Many craters smaller than  $\sim 175$  m (lower boundary of 250 m bin) are observed,

but these are not considered here due to the potential influence of secondary craters on the Mars production function [*McEwen et al.*, 2005]. On the basis of these seven craters, we can assign a model age of  $\sim 65$  Ma and a maximum age of  $\sim 115$  Ma for the fill surface based on the *Hartmann* 2004 production function. The same data, plotted cumulatively using the *Neukum* production function [*Hartmann and Neukum*, 2001; *Ivanov*, 2001], fall between the 10 and 100 Ma isochrons, with a fit of  $\sim 65$  Ma. On the basis of these crater counting results, we can confidently assign a late Amazonian age to the graben fill of less than a few hundred Ma, most likely  $<100$  Ma [*Shean et al.*, 2006]. As previously mentioned, the implications of such young ages for glaciation at Arsia Mons are significant, and may be consistent with our interpretation that the Arsia graben presently contains a significant amount of glacier ice beneath a debris cover.

## 6. Relationship Between Graben Fill and Smooth Facies Lobes

[43] We interpret the fill material within and immediately surrounding the large graben to represent the most recent phase of glaciation at Arsia Mons. This interpretation is supported by the (1) distinct morphology, (2) present thickness, (3) high elevation, and (4) location of the fill as the most proximal component of the fan-shaped deposit at Arsia. The flow ridges on the surface of the fill material were clearly influenced by the shape of the two alcoves along the southeastern wall, suggesting that graben fill formed during a separate phase of glaciation within the graben, instead of simply being preserved as residual material from a larger ice sheet at Arsia. In addition, recent age dating efforts using HRSC image data suggest that the graben fill is significantly younger than age estimates for the larger Arsia fan-shaped deposit [*Shean et al.*, 2006].

[44] On the basis of these observations, we can begin to address the question of how this young phase of glaciation fits into the overall glacial history of fan-shaped deposit formation at Arsia Mons and how some of the earlier phases might have been emplaced. Furthermore, these observations can be used to develop an understanding of how this local system would operate during extended periods with net glacial accumulation, potentially producing a significantly larger glacier that could fill and overflow the graben.

[45] Clues for understanding this type of activity can be found in the most proximal smooth facies lobes immediately to the northwest of the graben (pink unit in Figure 4; Figure 13). These features have been well-documented in the past [*Lucchitta*, 1981; *Zimelman and Edgett*, 1992; *Scott and Zimelman*, 1995; *Head and Marchant*, 2003] due to their striking morphology, lobate nature and numerous transverse, concentric surface ridges that are especially pronounced in the thicker, distal toes of the lobes. Many of these surface ridges are similar to those observed within the graben, while others appear to be composed predominantly of debris. In some locations, continuous ridges within the smooth facies can be mapped onto surrounding terrain where the smooth facies is no longer present (see arrow, Figure 13), providing yet another line of evidence suggesting that the smooth facies has experienced retreat [*Shean et al.*, 2006; *Head et al.*, manuscript in preparation, 2007].

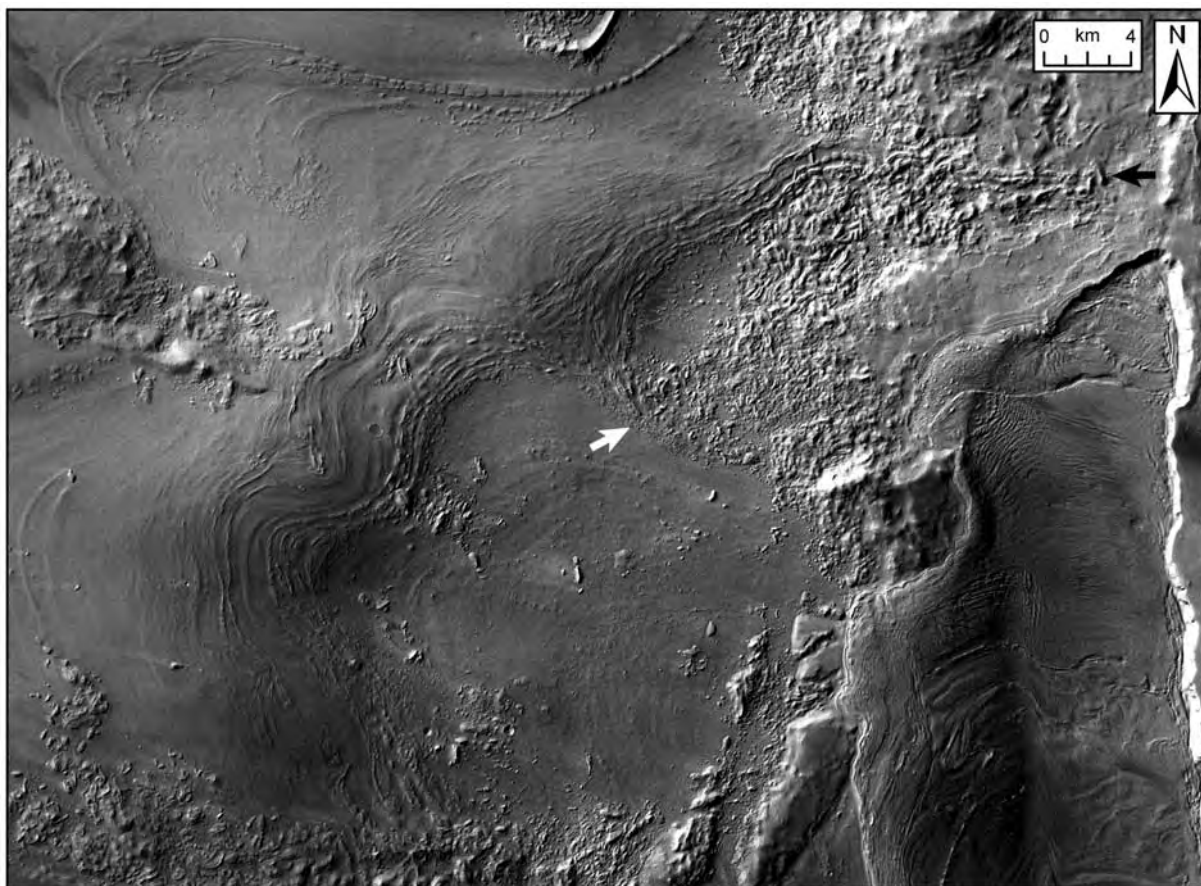


**Figure 13.** HRSC data (Orbits h1034 and h1045) showing the areas to the northwest of the large graben. The most proximal smooth facies lobes are delineated by their arcuate ridges, which appear highly concentric to the present margins of the graben fill lobes (see Figure 4). Note the distinctive “v” in the ridges (white arrow) that connects with a debris “trail” back to the topographic obstacle (~400 m relief) that separates lobes 1 and 2 on the present fill surface. It appears that this same obstacle separated the two smooth facies lobes that we suggest were sourced within the large graben. Note also the smooth facies ridges that appear to continue onto surfaces where the smooth facies is no longer present (black arrow in northeastern corner of image). This relationship is consistent with several other lines of evidence indicating that the smooth facies has experienced (or is currently experiencing) retreat since its initial emplacement.

[46] The ridges in the proximal lobes of the smooth facies (purple lines in Figure 4) were mapped from HRSC image data and as expected, the distribution of these ridges clearly delineates individual lobes of the smooth facies visible in MOLA topography (Figure 2). However, the most interesting discovery from this mapping is an apparent relationship between the smooth facies lobes and the fill material within and surrounding the Arsia graben (Figure 14).

[47] The ridges in the two smooth facies lobes closest to the graben fill are highly concentric to the current margins of lobes 1 and 2 (Figures 4, 13, and 14), which are separated by a large block of preexisting Arsia shield material (labeled T.O. in Figure 4). During filling and overflow of the graben, it appears that this block served as a topographic obstacle, impeding flow of the fill material to the northeast and splitting what would have been one large lobe into lobes 1 and 2. Following local slopes to the northwest of this obstacle, we encounter a point of convergence between the two most proximal smooth facies lobes (marked by “v-shaped” junctions of several ridges that point toward the

topographic obstacle, white arrow in Figure 13). A close examination of HRSC data shows that a line of debris connects the topographic obstacle and the point where the ridges on the two proximal smooth facies lobes converge (Figure 13). Furthermore, if we follow local slopes from the present margins of lobes 1 and 2 (Figure 4), we encounter the most proximal smooth facies lobes with ridges that are roughly normal to bed slopes (Figures 2 and 5).

[48] These observations provide compelling evidence that the most proximal lobes of the smooth facies had their origin in the large graben. Continuing to follow local slopes to the northwest, we encounter at least two additional pairs of slightly larger smooth facies lobes that are similarly concentric to the margins of the graben fill lobes, suggesting they may also have originated within the graben (Figures 1 and 2).

[49] The implications of these observations and correlations are significant for understanding the smooth facies and graben fill at Arsia Mons. We interpret the most proximal smooth facies lobes as the remnants of glacial lobes that had

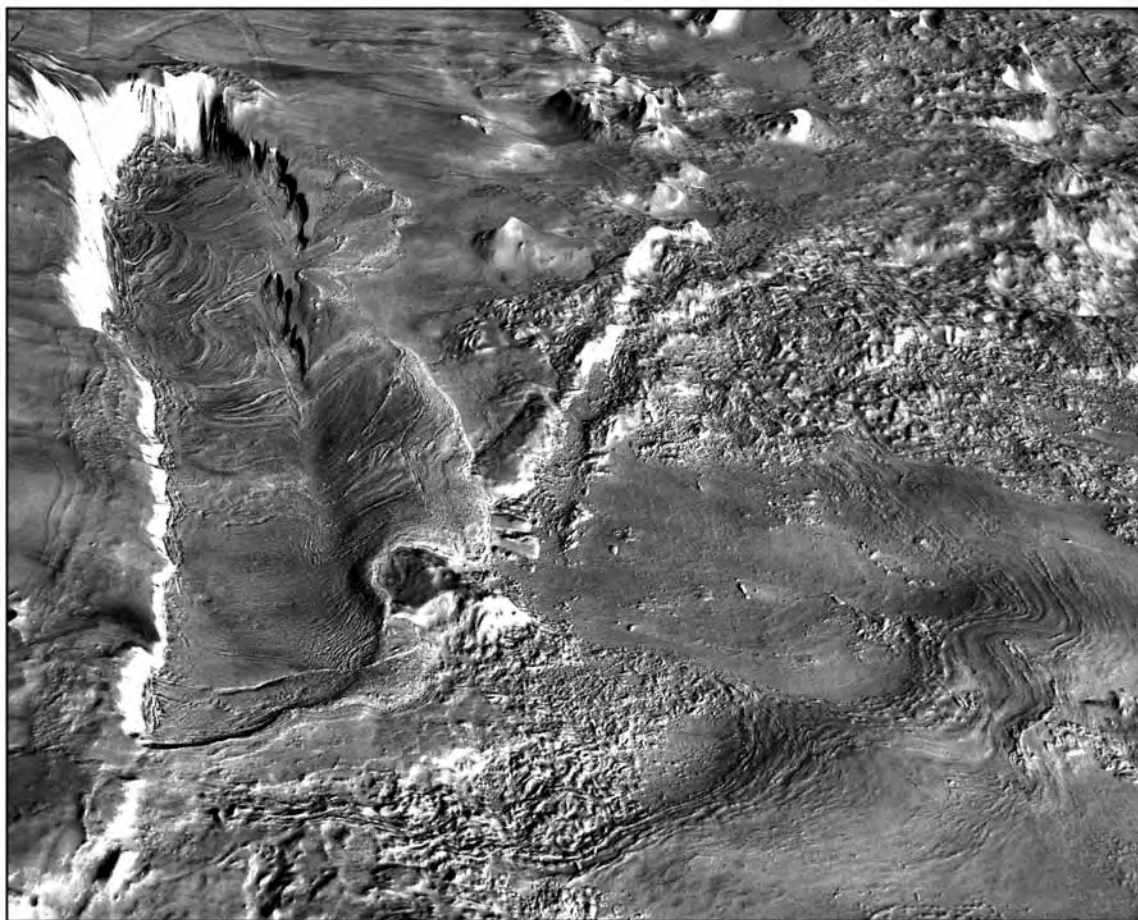


**Figure 14.** Three-dimensional perspective view of the large graben from the north with HRSC image data draped over MOLA topography (with areas near the graben draped over the improved implicit interpolation DEM described in Figure 5). Vertical exaggeration is 5 $\times$ .

their source within the graben. However, our interpretation suggests that these larger smooth facies lobes were formed before the graben fill lobes (lobes 1 and 2, Figure 4) that presently cover the northwestern graben rim. Unlike the conditions necessary to form the graben fill lobes, the glacial conditions that formed the larger smooth facies lobes were either more conducive to this style of glaciation (i.e., greater accumulation, less ablation, etc.) or persisted for a longer period of time. Alternatively, these larger smooth facies glaciers could have formed when a critical threshold due to the unique topography of the graben was exceeded, initiating much more rapid and expansive growth. The importance of topographically related thresholds in ice sheet initiation and growth has been well documented for terrestrial ice sheets [Payne and Sugden, 1990; Hulton and Sugden, 1997]. Regardless of the actual mechanism, these conditions allowed for more ice to accumulate within the graben and produced larger lobes that overflowed the graben walls and moved farther downslope to the northwest, eventually forming the proximal smooth facies lobes. The present deflated topography of the smooth facies lobes is consistent with their apparently older age, in contrast to the thick lobes of the relatively young graben fill.

[50] Thus far we have only considered the proximal smooth facies lobes and their apparent relationship to the graben fill. Additional smooth facies lobes that extend

hundreds of kilometers from the graben (red unit in Figure 1) appear to share a similar origin with the smaller smooth facies lobes. While it is difficult to precisely confirm the original source for these more extensive lobes, they are generally concentric to the more proximal smooth facies lobes, suggesting a similar source location. They could have formed due to initial localized accumulation within the Arsia graben during extended periods of greater ice accumulation, producing larger glacial lobes with greater areal coverage. This interpretation suggests that the concentric smooth facies lobes may represent a record of several distinct episodes of localized tropical mountain glaciation at Arsia Mons in the recent past.

## 7. Ice Sheet Models and Reconstruction Efforts

### 7.1. Present Graben Topography and Postglacial Modification

[51] The morphological evidence presented here provides several lines of evidence suggesting that the fill material within the large graben at Arsia is of glacial origin. Several independent lines of evidence show that the graben was completely filled with ice in the past, with subsequent overflow of the walls and observable retreat and ablation. In addition, the morphological observations of the fill material within the graben at Arsia Mons clearly indicate

northward flow away from the cirque-like alcoves along the southeastern graben wall. MOLA altimetry profiles along the longitudinal axis of the graben (Figure 2), however, show that the fill surface has a slight southward slope of  $\sim 0.3^\circ$ , sloping away from, not toward, the inferred flow direction (Figure 5). While this low surface slope is essentially flat, the profiles reveal an elevation difference of  $\sim 500$  m between the surface of the fill material near the northern and southern rim of the graben (Figure 5). This observation confirms that significant ice loss has occurred since the fill material overflowed the graben walls, and we now consider the magnitude and possible mechanisms for this loss.

[52] In order to assess the implications of the observed fill topography, we begin with the assumption that the graben, in some form, was present prior to glacier formation, or more specifically, that it did not initially form beneath an existing glacier (resulting in downdropping of an overlying column of glacial ice). This assumption is based on the following observations: (1) the graben fill is clearly superposed over the western graben rim, (2) the depositional ridges interpreted as drop moraines east of the graben are concentric to the present graben rim, and (3) the ridges and furrows on the surface of the graben fill define two lobes that originated within alcoves along the southeastern graben wall.

[53] On the basis of these observations suggesting pre-glacial graben formation, we consider a few scenarios that could potentially explain the evolution of the debris-covered glacier ice from initial deposition to its present topographic and morphologic configuration. The surface topography might be related to additional subsidence of a shallower graben floor, differential sublimation with greater ice loss in

the southern regions of the graben, or some combination of the two. Additional subsidence might result from ice loading and local stresses reactivating the faults that originally formed the graben. However, we also know that significant ice loss and retreat of the graben fill has occurred, so it is not unreasonable to consider the differential sublimation that might arise from debris cover anisotropy. This type of ablation is observed for terrestrial debris-covered glaciers, with greatest preservation in the distal regions beneath much thicker debris cover, in contrast to the abundant loss of relatively clean, exposed glacial ice near the accumulation zone leaving a characteristic “spoon-shaped hollow” or depression. There are difficulties with both of these scenarios; future efforts to understand initial graben formation mechanism(s) and advances in modeling sublimation under Martian conditions will help to improve our understanding.

## 7.2. Ice Sheet Modeling: Glacier Formation and Flow Within the Arsia Graben

[54] In order to try to answer some of these questions about the graben floor orientation and to better understand ice flow within the large graben at Arsia Mons, several model runs were executed using the University of Maine Ice Sheet Model (UMISM) [Fastook and Prentice, 1994; Huybrechts et al., 1996] and the results were compared to the observed features. For these simulations, the UMISM model was adjusted for Mars conditions (gravity, surface temperatures, basal heat flow, etc) and inputs for bed topography and ice surface topography were extracted from MOLA altimetric point data of the graben region (Figure 15). Several cases were considered for the bed topography by changing the slope of the graben floor while the graben walls and terrain surrounding the graben were kept constant.

**Figure 15.** (a) Longitudinal profiles of the four input bed definitions compared to the MOLA point data (Orbit 16499) for the large graben. Vertical exaggeration (VE) is  $45\times$ . Case 1 defines a shallow, flat bed that intersects the present graben fill surface at its highest point. Case 2 defines a sloped bed ( $\sim 0.3^\circ$  to the south) just beneath the present fill surface. Case 3 defines a deep, flat bed that intersects the present graben fill surface at its lowest point. Case 4 defines a sloped bed ( $\sim 0.3^\circ$  to the north) that intersects the graben fill at its lowest point. Each of these bed definitions was used for profile and map-plane simulations. (b) Longitudinal profiles showing the northward expansion of the glacier that would form after 1 Myr for bed topography cases 2–4. VE is  $45\times$ . The results of these initial trials show that the small slope variations of cases 2–4 have a small overall effect on the maximum northward expansion of ice within the graben. All model runs had the same initial inputs, with accumulation ( $+10$  mm/yr) along the entire southeastern wall of the graben and ablation ( $-1$  mm/yr) everywhere else. At 1 Myr, case 2 had noticeable overflow of the southwestern graben wall, case 3 had just begun to overflow the southwestern graben wall, and case 4 was still filling the graben with no overflow. None of these glaciers reached equilibrium by 1 Myr with the defined mass balance scheme (MB 0). (c) Map-plane model of ice thickness (m) after 1 Myr for the case 3 bed definition with the mass balance scheme described for Figure 15b. Contour interval is 100 m. Note how the ice has filled the deep portion of the graben and is only beginning to overflow the southwestern wall. The positive ice surface to the south of the graben is a result of the coarse definition of the positive accumulation along the southeastern walls and should be ignored. (d) Map-plane model of ice velocity (mm/yr) after  $\sim 0.5$  Myr for the case 3 bed definition with positive accumulation ( $+10$  mm/yr) limited only to the two alcoves on the southeastern graben wall and ablation ( $-0.01$  mm/yr) elsewhere. Contours show ice surface; colors represent ice velocity. Notice the development of a fast-moving “stream” of ice from the northern graben that matches the observed surface ridge patterns in HRSC image data. A second “stream” also extends from the southern alcove with a much smaller absolute velocity. This same velocity distribution was observed for nearly every model run with accumulation along the southeastern wall. (e) Map-plane model of ice thickness (m) after  $\sim 0.5$  Myr for the case 3 bed definition with the following mass balance scheme: positive accumulation ( $+10$  mm/yr) in the southeastern alcoves, positive accumulation ( $+5$  mm/yr) along the remainder of the eastern wall, positive accumulation ( $+2$  mm/yr) on the floor of the graben, zero net mass balance along the western wall, and ablation ( $-0.01$  mm/yr) on all other surface. This scenario shows significant overflow of the graben walls after  $\sim 0.5$  Myr due to the much greater accumulation rates. Note how the overflow to the northwest splits into two lobes due to the influence of the topographic obstacle (labeled T.O., see Figure 4), reproducing the presently observed distribution of graben fill.

A total of four cases for the graben floor were considered (Figure 15a) on the basis of the present fill topography, including (1) a shallow, flat floor at the maximum elevation of present fill surface (implying subsequent synglacial or postglacial graben subsidence), (2) a shallow, south-sloping floor just beneath the present fill surface ( $\sim 0.3^\circ$  slope, implying that the graben fill is very thin), (3) a deep, flat floor at the minimum elevation of present fill surface (implying that a  $\sim 500$  m thick wedge of fill is still present in the northern regions of the large graben), and (4) a deep, north-sloping floor ( $\sim 0.3^\circ$  slope, implying an even thicker extant fill wedge).

[55] The initial tests utilized a 2-D profile version of the model to assess the validity of these bed definitions on the basis of the current fill topography, assuming that the fill material was pure ice. The results of these initial tests show

that for all of the bed definitions, the fill material was stable within the graben and did not experience significant flow from its current orientation. Even when a “flow enhancement parameter” within the model was increased to 1000 times its nominal value for Mars conditions, the larger fill surface ridges experienced slight smoothing, but no backflow into the southern regions of the graben occurred. These initial results suggested that all the bed cases, including those with large thicknesses of preserved ice, were viable.

[56] After these initial tests, a series of additional model runs were designed to simulate glacier formation on an ice-free bedrock surface. However, due to the steep slopes of the graben walls ( $>25^\circ$  in places), the shallow-ice approximation of the 2-D profile model was no longer valid near the edges of the graben. This problem was reconsidered using the map-plane, 3-D version of the

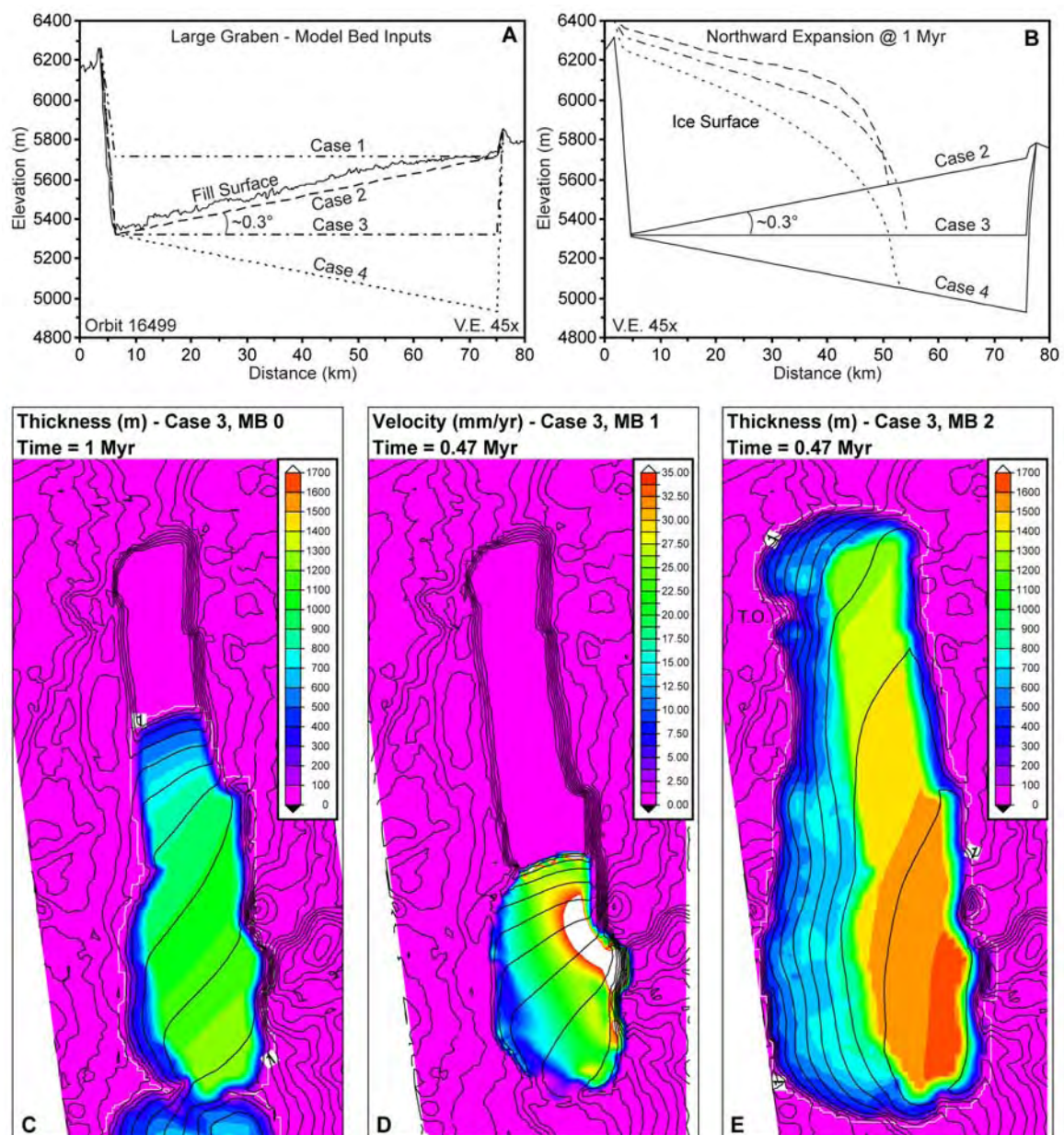


Figure 15

UMISM model, which was modified to correct the shallow-ice approximation.

[57] Each of the four bed topography cases (Figure 15a) was tested with identical initial parameters; accumulation (+10 mm/yr) was confined to the entire southeastern wall of the graben with ablation ( $-0.01$  mm/yr) at all other locations. The model was run for 1 Myr with a 10 Kyr time step. None of the cases reached steady state equilibrium by the end of this 1 Myr period for the defined mass balance. The first bed definition (case 1, Figure 15a) experienced significant overflow to the west of the graben early in the simulation, as would be expected for such a shallow floor. The results of the remaining model runs show that the small variation in the bed slopes ( $-0.3^\circ$  to  $+0.3^\circ$ ) for deeper graben floors do not significantly affect ice flow. The final northward expansion of ice within the graben was surprisingly similar for cases 2–4 (Figure 15b). None of these cases showed significant overflow to the west of the graben walls, although this was beginning to occur in case 2 near the observed location of lobe 3 (Figure 4). Velocity maps of the ice flow (e.g., Figure 15d) show that faster bands of ice extended from individual alcoves on the southeastern wall. In each case, these high-velocity “streams” displayed northward motion as the ice to the south grew sufficiently thick. This velocity distribution (Figure 15d) matches the locations of observed individual glaciers sourced at the alcoves along the southeastern graben wall that experienced significant northward flow.

[58] With this new understanding of how the graben floor topography would affect ice flow, a series of experiments were performed to test different initial mass balance schemes. The bed topography of case 3, with a deep, flat floor was held constant for these simulations, while the relative mass balance was varied within five locations across the scene, including the (1) two southeastern alcoves, (2) remainder of the eastern wall outside of southeastern alcoves, (3) graben floor, (4) western wall, and (5) surrounding terrain. Three initial mass balance schemes were considered, with (1) accumulation (+10 mm/yr) only within the two southeastern alcoves, ablation ( $-0.01$  mm/yr) on all other surfaces, (2) high accumulation within the alcoves (+10 mm/yr), less accumulation along the entire eastern wall (+5 mm/yr), slightly positive mass balance on the floor of the graben (+2 mm/yr), zero net mass balance on the western wall and ablation ( $-0.01$  mm/yr) elsewhere, and (3) high accumulation within the alcoves (+10 mm/yr), less accumulation along the entire eastern wall (+5 mm/yr), zero net mass balance on the floor and western wall of the graben with ablation ( $-0.01$  mm/yr) elsewhere. Each of these scenarios was allowed to run for 1 Myr, with a 10 Kyr time step. As with the first model runs, none reached equilibrium by the end of the run. In all of the runs, the glacier filled the graben, overflowed the western wall and advanced down local slopes to the west. The main differences between the runs were the timing, extent and general location of overflow. As expected, mass balance schemes 2 and 3 filled the graben and overflowed the entire western wall in a comparatively short time period, while the limited accumulation of mass balance scheme 1 (accumulation only in the southeastern alcoves) resulted in much later overflow. For all map-plane reconstructions with case 3 bed topography, initial overflow of the graben occurred along the southwest-

ern wall. This is consistent with observations of graben fill lobe 3 and drop moraines beyond the southwestern wall (Figure 4), but we do not observe proximal smooth facies lobes in these regions. Overflow along the northwestern graben wall eventually occurs for each model run, but only after significant overflow along the southwestern walls. This result partially stems from the fact that the fill lobes (1–3) to the west of the graben were not removed from the bed topography for these simulations. Thus the  $>250$  m thickness of lobe 2 (Figure 5) undoubtedly prevented initial overflow of the central and northern portion of the western graben wall until sufficient ice thicknesses within the graben were achieved. This large southwestern overflow may also suggest that the mass balance definitions in the models need refinement and/or that the actual floor of the graben during glacier formation had a greater northward slope than the case 3 bed definition.

[59] For the mass balance schemes (MB 2 and 3) with accumulation along the entire eastern wall, overflow to the northwest was also observed with splitting around the topographic obstacle identified in Figure 4 (Figure 15e). Finally, as with the initial model runs, high-velocity, northward ice “streams” were observed extending away from the two southeastern alcoves for each of the mass balance schemes tested (Figure 15d).

[60] In summary, these initial modeling efforts suggest that the observed  $\sim 0.3^\circ$  southward surface slope of the graben fill surface is not sufficient to cause backflow of the fill into the southern portion of the graben, and that small variations in the surface have little effect on the overall northward advance of a glacier sourced along the southeastern wall of the graben (Figure 15b). All cases experienced overflow of the western wall, with the greatest difference between the four cases tested being the timing of this western wall overflow (relatively rapid overflow for the shallower bed cases when compared to the deeper bed cases). Finally, high-velocity “streams” were observed extending northward from alcoves along the southeastern wall of the graben in all model runs. This northward flow was caused by filling of the southern graben, producing velocity distributions that match the observed arcuate ridge and furrow patterns of the two lobes on the fill surface.

## 8. Summary and Conclusions

[61] We interpret the fill material within large collapse features on the western flanks of Arsia Mons to be the depositional remains of the most recent phase of localized cold-based glaciation responsible for fan-shaped deposit production. The morphology of the features within the largest graben strongly support this interpretation: (1) the  $\sim 10$ – $30$  m high arcuate ridges and furrows on the graben fill surface are indicative of glacial flow and deformation, (2) these concentric ridges define two primary glacial lobes that can be traced for  $>30$  km from two cirque-like alcoves along the southeastern graben wall (interpreted as the primary accumulation zones and sources of debris for these glaciers), (3) the fill material and characteristic surface ridges are continuous across the  $200$ – $300$  m high western graben wall, forming a  $\sim 100$ – $250$  m thick lobe that extends  $\sim 5$ – $10$  km downslope onto the surrounding terrain, (4) several groups of concentric ridges around the

margins of the graben rim and lobes to the west of the graben appear to be drop moraines deposited during retreat of the glacier, and (5) the location and distribution of these lobes extending to the west and northwest of the graben (lobes 1–3, Figure 4) are highly concentric with the most proximal smooth facies lobes at Arsia, suggesting that the two are fundamentally related.

[62] Additional high-relief collapse features at similar elevations on the Arsia flank show further evidence for glaciation. These features are characterized by (1) dissected fill on their floors, (2) downslope concentric ridges interpreted as drop moraines, (3) debris fields with aligned boulders interpreted as till, and (4) patches of convex fill material interpreted as debris-covered glacial ice.

[63] These data provide insight into both glaciation and deglaciation processes at Arsia Mons and elsewhere on Mars, with features indicative of glacial advance, overflowing of valley margins, retreat during deglaciation (sublimation, down-wasting), and re-advance. Our results are consistent with the debris-covered glacier interpretation for the broader smooth facies at Arsia Mons and suggest that the lobes of the smooth facies may represent more recent phases of glaciation than that which produced the large fan-shaped deposit. It appears that at least the most proximal smooth facies lobes were originally sourced within the large graben, forming when debris-covered glacier(s) filled the graben, overflowed the graben walls, and advanced for at least  $\sim 80$  km down local slopes. Finally, these smooth facies lobes are older and more degraded than the present graben fill lobes, allowing us to further refine the stratigraphy and sequence of glaciation responsible for producing the Arsia fan-shaped deposit.

[64] Debris-covered glaciers are valuable morphological indicators of climate change on Earth. The features high on the flanks of Arsia Mons are similar in scale and morphology to cold-based, debris-covered glaciers observed in the Dry Valleys of Antarctica. Age estimates of  $\sim 35$ – $115$  Ma (model age of  $\sim 65$  Ma) for the fill in the large Arsia graben suggest that conditions conducive to forming these glaciers via atmospheric precipitation [Forget et al., 2006] were present in recent geologic history and that those conditions are no longer present, resulting in retreat and sublimation of the glacial ice. The conditions necessary to form these features are believed to involve higher obliquities ( $>45^\circ$ ) with equatorward frost point migration and volatile transport form the poles to the equatorial regions [Richardson and Wilson, 2002; Head and Marchant, 2003; Mischna et al., 2003; Shean et al., 2005], specifically to the western flanks of the Tharsis Montes [Forget et al., 2006]. Thus we believe that these conditions had to be present for a time period sufficient to at least form the youngest graben fill lobes within the past  $\sim 115$  Myr, providing additional evidence for recent climate change on Mars.

[65] MOLA topography data suggest that  $\sim 100$ – $300$  m of ice is still preserved at Arsia Mons beneath a debris cover within the large graben and in the surrounding smooth facies lobes. This observation suggests that in these locations, equatorial ice has been preserved for tens to potentially  $\sim 100$  Myr beneath a relatively thin debris cover. This stability has implications for sublimation processes on Mars and the importance of a debris cover for ice preservation on the surface [Helbert et al., 2005]. Initial results from the

Berlin Mars Near-Surface Thermal Model [Helbert et al., 2005] suggest that within the large graben, ice could survive beneath a debris cover that is only a few meters thick for at least 50 Myr [Helbert et al., 2006].

[66] Specific questions that deserve further attention include the following: (1) When and how did the high-altitude,  $\sim 70 \times 8$  km large graben originally form? (2) What processes are responsible for the present graben fill topography? (3) Could the large graben serve as a local accumulation area and/or debris source for a much larger glacier at Arsia Mons? (4) What processes are responsible for forming the arcuate ridge and furrow morphology observed on the graben fill surface and how is it related to recent climate change on Mars? Additional data from Mars, terrestrial analog studies, and modeling efforts will help to answer some of these important questions in the future.

[67] **Acknowledgments.** We thank the HRSC Experiment Teams at DLR Berlin and Freie Universitaet Berlin as well as the Mars Express Project Teams at ESTEC and ESOC for their successful planning and acquisition of data as well as for making the processed data available to the HRSC Team. We acknowledge the effort of the HRSC Co-Investigator Team members and their associates, who have contributed to this investigation in the preparatory phase and in scientific discussions within the Team. We would also like to thank Prabhat for HRSC/MOLA DTM generation and C. Fassett, J. Dickson, J. Helbert, P. Russell, and M. Kreslavsky for productive discussions and assistance. We thank D. Sugden and an anonymous reviewer for their insightful comments and suggestions for improvements. NASA grants to J.W.H. (Mars Data Analysis Program, NNG04GJ996; Mars Express High Resolution Stereo Camera Team participation, JPL 1237163; Applied Information System Research Program, NNG05GA61G) and National Science Foundation grant OPP-0338291 to D.R.M. helped to support this research and are gratefully acknowledged.

## References

- Ackert, R. P. (1998), A rock glacier/debris-covered glacier system at Galena Creek, Absaroka Mountains, Wyoming, *Geogr. Ann., Ser. A*, 80(3–4), 267–276.
- Arcone, S. A., M. L. Prentice, and A. J. Delaney (2002), Stratigraphic profiling with ground-penetrating radar in permafrost: A review of possible analogs for Mars, *J. Geophys. Res.*, 107(E11), 5108, doi:10.1029/2002JE001906.
- Arfstrom, J., and W. K. Hartmann (2005), Martian flow features, moraine-like ridges, and gullies: Terrestrial analogs and interrelationships, *Icarus*, 174(2), 321–335.
- Atkins, C. B., P. J. Barrett, and S. R. Hicock (2002), Cold glaciers erode and deposit: Evidence from Allan Hills, Antarctica, *Geology*, 30(7), 659–662.
- Barsch, D. (1996), *Rock Glaciers: Indicators for the Present and Former Geocology in High Mountain Environments*, 331 pp., Springer, New York.
- Benn, D. I., and D. J. A. Evans (1998), *Glaciers and Glaciation*, 734 pp., Edward Arnold, London.
- Berman, D. C., W. K. Hartmann, D. A. Crown, and V. R. Baker (2005), The role of arcuate ridges and gullies in the degradation of craters in the Newton Basin region of Mars, *Icarus*, 178(2), 465–486.
- Bickerton, R. W., and J. A. Matthews (1993), “Little Ice Age” variations of outlet glaciers from the Jostedalbreen ice-cap, southern Norway: A regional lichenometric-dating study of ice-marginal moraine sequences and their climatic significance, *J. Quat. Sci.*, 8(1), 45–66.
- Bozhinskiy, A. N., M. S. Krass, and V. V. Popovnin (1986), Role of debris cover in the thermal physics of glaciers, *J. Glaciol.*, 32(111), 255–266.
- Brook, E. J., M. D. Kurz, J. R. P. Ackert, G. H. Denton, E. T. Brown, G. M. Raisbeck, and F. You (1993), Chronology of Taylor Glacier advances in Arena Valley, Antarctica, using in situ cosmogenic  $^3\text{He}$  and  $^{10}\text{Be}$ , *Quat. Res.*, 39(1), 11–23.
- Carr, M. H. (1996), *Water on Mars*, 229 pp., Oxford Univ. Press, New York.
- Carr, M. H. (2001), Mars Global Surveyor observations of Martian fretted terrain, *J. Geophys. Res.*, 106(E10), 23,571–23,594.
- Cas, R. A. F., and J. V. Wright (1987), *Volcanic Successions, Modern and Ancient: A Geological Approach to Processes, Products and Successions*, 528 pp., Allen and Unwin, St Leonards, NSW, Australia.

- Chuang, F. C., and D. A. Crown (2005), Surface characteristics and degradation history of debris aprons in the Tempe Terra/Mareotis Fossae region of Mars, *Icarus*, 179(1), 24–42.
- Colaprete, A., and B. M. Jakosky (1998), Ice flow and rock glaciers on Mars, *J. Geophys. Res.*, 103(E3), 5897–5909.
- Cuffey, K. M., H. Conway, A. M. Gades, B. Hallet, R. Lorrain, J. P. Severinghaus, E. J. Steig, B. Vaughn, and J. W. C. White (2000), Entrainment at cold glacier beds, *Geology*, 28(4), 351–354.
- Degenhardt, J. J., Jr., and J. R. Giardino (2003), Subsurface investigation of a rock glacier using ground-penetrating radar: Implications for locating stored water on Mars, *J. Geophys. Res.*, 108(E4), 8036, doi:10.1029/2002JE001888.
- Dickson, J. L., J. W. Head III, R. L. Parsons, G. Neukum, and the HRSC Co-Investigator Team (2005), Arsia Mons flank pit craters and valleys: Modification by downslope movement processes, *Lunar Planet. Sci.* [CD-ROM], XXXVI, Abstract 1790.
- Fastook, J. L., and M. Prentice (1994), A finite-element model of Antarctica: Sensitivity test for meteorological mass-balance relationship, *J. Glaciol.*, 40(134), 167–175.
- Forget, F., R. M. Haberle, F. Montmessin, B. Levrard, and J. W. Head (2006), Formation of glaciers on Mars by atmospheric precipitation at high obliquity, *Science*, 311(5759), 368–371.
- Garlick, G. D. (1988), Evidence for the derivation of Martian glaciers from ground ice, *Geol. Soc. Am. Abstr. Programs*, 20, 162, Abstract 24326.
- Garvin, J. B., S. E. H. Sakimoto, J. J. Frawley, and C. Schnetzler (2000), North polar region craterforms on Mars: Geometric characteristics from the Mars Orbiter Laser Altimeter, *Icarus*, 144(2), 329–352.
- Garvin, J. B., J. W. Head, D. R. Marchant, and M. A. Kreslavsky (2006), High-latitude cold-based glacial deposits on Mars: Multiple superposed drop moraines in a crater interior at 70°N latitude, *Meteorit. Planet. Sci.*, 41(10), 1659–1674.
- Gillespie, A. R., D. R. Montgomery, and A. Mushkin (2005), Are there active glaciers on Mars?, *Nature*, 438(7069), doi:10.1038/nature04358.
- Gosse, J. C., J. Klein, E. B. Evenson, B. Lawn, and R. Middleton (1995), Beryllium-10 dating of the duration and retreat of the last Pinedale glacial sequence, *Science*, 268(5215), 1329–1333.
- Goudy, C. L., and R. A. Schultz (2005), Dike intrusions beneath grabens south of Arsia Mons, Mars, *Geophys. Res. Lett.*, 32, L05201, doi:10.1029/2004GL021977.
- Haberle, R. M., F. Montmessin, F. Forget, B. Levrard, J. W. Head, and J. Laskar (2004), GCM simulations of tropical ice accumulations: Implications for cold-based glaciers, *Lunar Planet. Sci.* [CD-ROM], XXXV, Abstract 1711.
- Hamilton, S. J., and W. B. Whalley (1995), Rock glacier nomenclature: A re-assessment, *Geomorphology*, 14, 73–80.
- Hartmann, W. K. (2005), Martian cratering 8: Isochron refinement and the chronology of Mars, *Icarus*, 174(2), 294–320.
- Hartmann, W. K., and G. Neukum (2001), Cratering chronology and the evolution of Mars, *Space Sci. Rev.*, 96, 165–194.
- Hartmann, W. K., M. Malin, A. McEwen, M. Carr, L. Soderblom, P. Thomas, E. Danielson, P. James, and V. Joseph (1999), Evidence for recent volcanism on Mars from crater counts, *Nature*, 397(6720), 586–589.
- Hassinger, J. M., and P. A. Mayewski (1983), Morphology and dynamics of the rock glaciers in southern Victoria Land, Antarctica, *Arctic Alpine Res.*, 15(3), 351–368.
- Hauber, E., S. Van Gasselt, B. Ivanov, S. Werner, J. W. Head, G. Neukum, R. Jaumann, R. Greeley, K. L. Mitchell, and P. Muller (2005), Discovery of a flank caldera and very young glacial activity at Hecates Tholus, Mars, *Nature*, 434(7031), 356–361.
- Head, J. W., and D. R. Marchant (2003), Cold-based mountain glaciers on Mars: Western Arsia Mons, *Geology*, 31(7), 641–644.
- Head, J. W., and L. Wilson (2002), Mars: A review and synthesis of general environments and geological settings of magma-H<sub>2</sub>O interactions, in *Volcano-Ice Interaction on Earth and Mars*, edited by J. L. Smellie and M. G. Chapman, *Geol. Soc. Spec. Publ.*, 202, 27–57.
- Head, J. W., J. F. Mustard, M. A. Kreslavsky, R. E. Milliken, and D. R. Marchant (2003), Recent ice ages on Mars, *Nature*, 426(6968), 797–802.
- Head, J. W., et al. (2005a), Tropical to mid-latitude snow and ice accumulation, flow and glaciation on Mars, *Nature*, 434(7031), 346–351.
- Head, J. W., et al. (2005b), Head et al. reply, *Nature*, 438(7069), doi:10.1038/nature04357.
- Head, J. W., D. R. Marchant, M. C. Agnew, C. I. Fassett, and M. A. Kreslavsky (2006), Extensive valley glacier deposits in the northern mid-latitudes of Mars: Evidence for Late Amazonian obliquity-driven climate change, *Earth Planet. Sci. Lett.*, 241(3–4), 663–671.
- Helbert, J., D. Reiss, E. Hauber, and J. Benkhoff (2005), Limits on the burial depth of glacial ice deposits on the flanks of Hecates Tholus, Mars, *Geophys. Res. Lett.*, 32, L17201, doi:10.1029/2005GL023712.
- Helbert, J., J. W. Head, D. R. Marchant, D. E. Shean, and M. Kreslavsky (2006), First prospecting for ice in the flank deposit at Arsia Mons, *Lunar Planet. Sci.* [CD-ROM], XXXVII, Abstract 1371.
- Howard, A. D. (2003), Tongue ridges and rumpled crater floors in mid-southern-latitude Martian craters, *Lunar Planet. Sci.* [CD-ROM], XXXIV, Abstract 2073.
- Hulton, N., and D. Sugden (1997), Dynamics of mountain ice caps during glacial cycles: The case of Patagonia, *Ann. Glaciol.*, 24, 81–89.
- Huybrechts, P., et al. (1996), The EISMINT benchmarks for testing ice-sheet models, *Ann. Glaciol.*, 23, 1–14.
- Ivanov, B. A. (2001), Mars/Moon cratering rate ratio estimates, *Space Sci. Rev.*, 96, 87–104.
- Kaab, A., and M. Weber (2004), Development of transverse ridges on rock glaciers: Field measurements and laboratory experiments, *Permafrost Periglacial Processes*, 15(4), 379–391.
- Konrad, S. K., N. F. Humphrey, E. J. Steig, D. H. Clark, N. Potter Jr., and W. T. Pfeffer (1999), Rock glacier dynamics and paleoclimatic implications, *Geology*, 27(12), 1131–1134.
- Kowalewski, D. E., D. R. Marchant, J. S. Levy, and J. W. Head (2006), Quantifying low rates of summertime sublimation for buried glacier ice in the Beacon Valley, Antarctica, *Antarct. Sci.*, 18(3), 421–428.
- Kreslavsky, M. A., J. W. Head, and D. R. Marchant (2007), Periods of active permafrost layer formation during the geological history of Mars: Implications for circum-polar and mid-latitude surface processes, *Planet. Space Sci.*, in press.
- Laskar, J., B. Levrard, and J. F. Mustard (2002), Orbital forcing of the Martian polar layered deposits, *Nature*, 419(6905), 375–377.
- Laskar, J., A. C. M. Correia, M. Gastineau, F. Joutel, B. Levrard, and P. Robutel (2004), Long term evolution and chaotic diffusion of the insolation quantities of Mars, *Icarus*, 170(2), 343–364.
- Levy, J., D. R. Marchant, and J. W. Head (2006), Distribution and origin of patterned ground on Mullins Valley debris-covered glacier, Antarctica: The roles of ice flow and sublimation, *Antarct. Sci.*, 18, 385–397, doi:10.1017/S0954102006000435.
- Loewenherz, D. S., C. J. Lawrence, and R. L. Weaver (1989), On the development of transverse ridges on rock glaciers, *J. Glaciol.*, 35(12), 383–391.
- Lorrey, A. M. (2002), Distribution of patterned ground and surficial deposits on a debris-covered glacier surface in Mullins Valley and Upper Beacon, Master's thesis, Univ. of Maine, Orono.
- Lorrey, A. M. (2005), Multiple remnant glaciers preserved in Beacon Valley, Antarctica, *Glacial Geol. Geomorphol.*, rp02/2005. (Available at [http://www.openj-gate.com/ArticleList.asp?Source=1&Journal\\_ID=101772](http://www.openj-gate.com/ArticleList.asp?Source=1&Journal_ID=101772))
- Lucchitta, B. K. (1981), Mars and Earth: Comparison of cold-climate features, *Icarus*, 45, 264–303.
- Lucchitta, B. K. (1984), Ice and debris in the fretted terrain, Mars, *Proc. Lunar Planet. Sci. Conf. 14th*, Part 2, *J. Geophys. Res.*, 89, suppl., B409–B418.
- MacClune, K. L., A. G. Fountain, J. S. Kargel, and D. R. MacAyeal (2003), Glaciers of the McMurdo dry valleys: Terrestrial analog for Martian polar sublimation, *J. Geophys. Res.*, 108(E4), 5031, doi:10.1029/2002JE001878.
- Mahaney, W. C., J. M. Dohm, V. R. Baker, H. E. Newsom, D. Malloch, R. G. V. Hancock, I. Campbell, D. Sheppard, and M. W. Milner (2001), Morphogenesis of Antarctic paleosols: Martian analogue, *Icarus*, 154(1), 113–130.
- Mangold, N. (2003), Geomorphic analysis of lobate debris aprons on Mars at Mars Orbiter Camera scale: Evidence for ice sublimation initiated by fractures, *J. Geophys. Res.*, 108(E4), 8021, doi:10.1029/2002JE001885.
- Marchant, D. R., and J. W. Head (2003), Tongue-shaped lobes on Mars: Morphology, nomenclature, and relation to rock glacier deposits (abstract), paper presented at Sixth International Conference on Mars, Lunar and Planet. Inst., Pasadena, Calif.
- Marchant, D. R., G. H. Denton, J. G. Bockheim, S. C. Wilson, and A. R. Kerr (1994), Quaternary changes in level of the upper Taylor Glacier, Antarctica: Implications for paleoclimate and East Antarctic Ice Sheet dynamics, *Boreas*, 23(1), 29–43.
- Marchant, D. R., A. R. Lewis, W. M. Phillips, E. J. Moore, R. A. Souchez, G. H. Denton, D. E. Sugden, N. Potter, and G. P. Landis (2002), Formation of patterned ground and sublimation till over Miocene glacier ice in Beacon Valley, southern Victoria Land, Antarctica, *Geol. Soc. Am. Bull.*, 114(6), 718–730.
- McEwen, A. S., B. S. Preblich, E. P. Turtle, N. A. Artemieva, M. P. Golombek, M. Hurst, R. L. Kirk, D. M. Burr, and P. R. Christensen (2005), The rayed crater Zunil and interpretations of small impact craters on Mars, *Icarus*, 176(2), 351–381.

- McGovern, P. J., and S. C. Solomon (1993), State of stress, faulting, and eruption characteristics of large volcanoes on Mars, *J. Geophys. Res.*, *98*(E12), 23,553–23,579.
- Milkovich, S. M., and J. W. Head III (2005), North polar cap of Mars: Polar layered deposit characterization and identification of a fundamental climate signal, *J. Geophys. Res.*, *110*, E01005, doi:10.1029/2004JE002349.
- Milkovich, S. M., J. W. Head, and D. R. Marchant (2006), Debris-covered piedmont glaciers along the northwest flank of the Olympus Mons scarp: Evidence for low-latitude ice accumulation during the Late Amazonian of Mars, *Icarus*, *181*(2), 388–407.
- Milliken, R. E., J. F. Mustard, and D. L. Goldsby (2003), Viscous flow features on the surface of Mars: Observations from high-resolution Mars Orbiter Camera (MOC) images, *J. Geophys. Res.*, *108*(E6), 5057, doi:10.1029/2002JE002005.
- Mischna, M. A., M. I. Richardson, R. J. Wilson, and D. J. McCleese (2003), On the orbital forcing of Martian water and CO<sub>2</sub> cycles: A general circulation model study with simplified volatile schemes, *J. Geophys. Res.*, *108*(E6), 5062, doi:10.1029/2003JE002051.
- Montesi, L. G. J. (2001), Concentric dikes on the flanks of Pavonis Mons: Implications for the evolution of Martian shield volcanoes and mantle plumes, in *Mantle Plumes: Their Identification Through Time*, edited by R. E. Ernst and K. L. Buchan, *Spec. Pap. Geol. Soc. Am.*, *352*, 165–181.
- Mouginis-Mark, P. J. (2002), Prodigious ash deposits near the summit of Arsia Mons volcano, Mars, *Geophys. Res. Lett.*, *29*(16), 1768, doi:10.1029/2002GL015296.
- Nakawo, M., and B. Rana (1999), Estimate of ablation rate of glacier ice under a supraglacial debris layer, *Geogr. Ann., Ser. A*, *81*(4), 695–701.
- Nakawo, M., and G. J. Young (1982), Estimate of glacier ablation under a debris layer from surface temperature and meteorological variables, *J. Glaciol.*, *28*(98), 29–34.
- Neukum, G., et al. (2004), Recent and episodic volcanic and glacial activity on Mars revealed by the High Resolution Stereo Camera, *Nature*, *432*(7020), 971–979.
- Parsons, R. L., and J. W. Head (2004), Ascraeus Mons, Mars: Characterization and interpretation of the fan-shaped deposit on its western flank, *Lunar Planet. Sci.* [CD-ROM], XXXV, Abstract 1776.
- Payne, A., and D. Sugden (1990), Topography and ice sheet growth, *Earth Surf. Processes Landforms*, *15*, 625–639.
- Perron, J. T., W. E. Dietrich, A. D. Howard, J. A. McKean, and J. R. Pettinga (2003a), Ice-driven creep on Martian debris slopes, *Geophys. Res. Lett.*, *30*(14), 1747, doi:10.1029/2003GL017603.
- Perron, J. T., A. D. Howard, and W. E. Dietrich (2003b), Viscous flow of ice-rich crater fill deposits and periodic formation of proglacial ramparts: A climate record? (abstract), paper presented at Sixth International Conference on Mars, Lunar and Planet. Inst., Pasadena, Calif.
- Potter, N. (1972), Ice-cored rock glacier, Galena Creek, Northern Absaroka Mountains, Wyoming, *Geol. Soc. Am. Bull.*, *83*(10), 3025–3058.
- Potter, N., E. J. Steig, D. H. Clark, M. A. Speece, G. M. Clark, and A. B. Updike (1998), Galena Creek rock glacier revisited—new observations on an old controversy, *Geogr. Ann., Ser. A*, *80*(3–4), 251–265.
- Rea, B. R., W. B. Whalley, T. S. Dixon, and J. E. Gordon (1999), Plateau icefields as contributing areas to valley glaciers and the potential impact on reconstructed ELAs: A case study from the Lyngen Alps, North Norway, *Ann. Glaciol.*, *28*, 97–102.
- Richardson, M. I., and R. J. Wilson (2002), Investigation of the nature and stability of the Martian seasonal water cycle with a general circulation model, *J. Geophys. Res.*, *107*(E5), 5031, doi:10.1029/2001JE001536.
- Rignot, E., B. Hallet, and A. Fountain (2002), Rock glacier surface motion in Beacon Valley, Antarctica, from synthetic-aperture radar interferometry, *Geophys. Res. Lett.*, *29*(12), 1607, doi:10.1029/2001GL013494.
- Russell, P. S., and J. W. Head (2005), Circum-polar craters with interior deposits on Mars: Polar region geologic, volatile, and climate history with implications for ground ice signatures in Arabia Terra, *Lunar Planet. Sci.* [CD-ROM], XXXVI, Abstract 1541.
- Russell, P. S., J. W. Head, and M. H. Hecht (2003), Evolution of volatile-rich crater interior deposits on Mars (abstract), paper presented at Sixth International Conference on Mars, Lunar and Planet. Inst., Pasadena, Calif.
- Scott, D. H., and J. R. Zimbelman (1995), Geologic map of Arsia Mons Volcano, Mars, *U. S. Geol. Surv. Geol. Invest. Ser., Map I-2480*.
- Scott, D. H., J. M. Dohm, and J. R. Zimbelman (1998), Geologic map of Pavonis Mons Volcano, Mars, *U. S. Geol. Surv. Geol. Invest. Ser., Map I-2561*.
- Scott, E. D., and L. Wilson (2002), Plinian eruptions and passive collapse events as mechanisms of formation for Martian pit chain craters, *J. Geophys. Res.*, *107*(E4), 5020, doi:10.1029/2000JE001432.
- Shean, D. E., J. W. Head, and D. R. Marchant (2005), Origin and evolution of a cold-based tropical mountain glacier on Mars: The Pavonis Mons fan-shaped deposit, *J. Geophys. Res.*, *110*, E05001, doi:10.1029/2004JE002360.
- Shean, D. E., J. W. Head, M. Kreslavsky, G. Neukum, and HRSC Co-Investigator Team (2006), When were glaciers present in Tharsis? Constraining age estimates for the Tharsis Montes fan-shaped deposits, *Lunar Planet. Sci.* [CD-ROM], XXXVII, Abstract 2092.
- Shean, D. E., D. R. Marchant, and J. W. Head (2007), Shallow seismic surveys and ice thickness estimates of the Mullins Valley debris-covered glacier, McMurdo Dry Valleys, Antarctica, *Antarct. Sci.*, in press.
- Squyres, S. W. (1979), The distribution of lobate debris aprons and similar flows on Mars, *J. Geophys. Res.*, *84*(B14), 8087–8096.
- Squyres, S. W. (1989), Urey Prize Lecture: Water on Mars, *Icarus*, *79*, 229–288.
- Squyres, S. W., and M. H. Carr (1986), Geomorphic evidence for the distribution of ground ice on Mars, *Science*, *231*(4735), 249–252.
- Staiger, J. W., D. R. Marchant, J. M. Schaefer, P. Oberholzer, J. V. Johnson, A. R. Lewis, and K. M. Swanger (2006), Plio-Pleistocene history of Ferrar Glacier, Antarctica: Implications for climate and ice sheet stability, *Earth Planet. Sci. Lett.*, *243*, 489–503.
- Vanden Heuvel, B. (2002), Surficial geology and geomorphology of the western Olympus Range, Antarctica: Implications for ice-sheet history, MS thesis, 107 pp., Univ. of Maine, Orono.
- Wahrhaftig, C., and A. Cox (1959), Rock glaciers in the Alaska Range, *Geol. Soc. Am. Bull.*, *70*(4), 383–436.
- Walter, T. R., and V. R. Troll (2001), Formation of caldera periphery faults: An experimental study, *Bull. Volcanol.*, *63*(2–3), 191–203.
- Wentworth, S. J., E. K. Gibson, M. A. Velbel, and D. S. McKay (2005), Antarctic Dry Valleys and indigenous weathering in Mars meteorites: Implications for water and life on Mars, *Icarus*, *174*(2), 383–395.
- Werner, S. (2006), Major aspects of the chronostratigraphy of geologic evolutionary history of Mars, Ph.D. thesis, 160 pp., Freie Univ. Berlin, Berlin.
- Whalley, W. B., and F. Azizi (1994), Rheological models of active rock glaciers: Evaluation, critique and a possible test, *Permafrost Periglacial Processes*, *5*, 37–51.
- Whalley, W. B., and F. Azizi (2003), Rock glaciers and protalus landforms: Analogous forms and ice sources on Earth and Mars, *J. Geophys. Res.*, *108*(E4), 8032, doi:10.1029/2002JE001864.
- Whalley, W. B., and H. E. Martin (1992), Rock glaciers, II: Models and mechanisms, *Prog. Phys. Geogr.*, *16*, 127–186.
- White, S. E. (1976), Rock glaciers and block fields, review and new data, *Quat. Res.*, *6*, 77–97.
- Williams, R. S. (1978), Geomorphic processes in Iceland and on Mars: A comparative appraisal from orbital images, *Geol. Soc. Am. Abstr. Programs*, *10*, 517.
- Wilson, L., and J. W. Head (1994), Mars: Review and analysis of volcanic eruption theory and relationships to observed landforms, *Rev. Geophys.*, *32*(3), 221–263.
- Wilson, L., and J. W. Head III (2002a), Tharsis-radial graben systems as the surface manifestation of plume-related dike intrusion complexes: Models and implications, *J. Geophys. Res.*, *107*(E8), 5057, doi:10.1029/2001JE001593.
- Wilson, L., and J. W. Head (2002b), Heat transfer and melting in subglacial basaltic volcanic eruptions: Implications for volcanic deposit morphology and meltwater volumes, in *Volcano-Ice Interaction on Earth and Mars*, edited by J. L. Smellie and M. G. Chapman, *Geol. Soc. Spec. Publ.*, *202*, 5–26.
- Wilson, L., and J. W. Head III (2004), Evidence for a massive phreatomagmatic eruption in the initial stages of formation of the Mangala Valles outflow channel, Mars, *Geophys. Res. Lett.*, *31*, L15701, doi:10.1029/2004GL020322.
- Zimbelman, J. R., and K. S. Edgett (1992), The Tharsis Montes, Mars: Comparison of volcanic and modified landforms, *Proc. Lunar Planet. Sci. Conf. 22nd*, 31–44.

J. L. Fastook, Department of Computer Science, University of Maine, 223 Neville Hall, Orono, ME 04469, USA.

J. W. Head, III Department of Geological Sciences, Brown University, Box 1846, Providence, RI 02912, USA. (james\_head@brown.edu)

D. R. Marchant and D. E. Shean, Department of Earth Science, Boston University, 675 Commonwealth Avenue, Boston, MA 02215, USA. (dshean@bu.edu)